NASA CR 121194

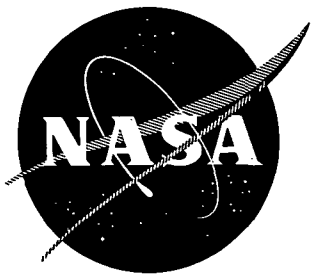


# *Theoretical Analysis of a Rotating Two Phase Detonation in a Rocket Motor*



by

I-wu Shen
T. C. Adamson, Jr.

*prepared for*

NATIONAL AERONAUTICS AND SPACE ADMINISTRATION
NASA Lewis Research Center
Grant NGL 23-005-336
R. J. Priem, Project Manager

*March 1973*

THE UNIVERSITY OF MICHIGAN
Department of Aerospace Engineering
Ann Arbor, Michigan

NASA CR 121194

# THEORETICAL ANALYSIS OF A ROTATING TWO PHASE DETONATION IN A ROCKET MOTOR

I-wu Shen

T. C. Adamson, Jr.

The University of Michigan
Department of Aerospace Engineering
Ann Arbor, Michigan 48104

prepared for

National Aeronautics and Space Administration
NASA Lewis Research Center
Grant NGL 23-005-336
R. J. Priem, Project Manager

March 1973

TABLE OF CONTENTS

## ABSTRACT

Tangential mode, non-linear wave motion in a liquid propellant rocket engine is studied, using a two phase detonation wave as the reaction model. Because the detonation wave is followed immediately by expansion waves, due to the side relief in the axial direction, it is a Chapman-Jouguet wave. The strength of this wave, which may be characterized by the pressure ratio across the wave, as well as the wave speed and the local wave Mach number, are related to design parameters such as the contraction ratio, chamber speed of sound, chamber diameter, propellant injection density and velocity, and the specific heat ratio of the burned gases. In addition, the distribution of flow properties along the injector face can be computed. Numerical calculations show favorable comparison with experimental findings. Finally, the effects of drop size are discussed and a simple criterion is found to set the lower limit of validity of this "strong wave" analysis.

## LIST OF FIGURES

## NOMENCLATURE

| | |
|---|---|
| A | area |
| a | speed of sound |
| B | function of Mach number, $M_o$, defined by Eq. (5) |
| $c_p$ | specific heat at constant pressure |
| d | diameter |
| f | oxidizer to fuel mass flow ratio ($= \dot{m}_o/\dot{m}_f$) |
| h | specific enthalpy |
| H | total enthalpy in the wave fixed coordinate system |
| $\ell$ | thickness |
| L | length and wave length |
| $\dot{m}$ | mass flow rate |
| M | Mach number |
| p | pressure |
| q | velocity |
| Q | heat release ($= h_d - h^o$) |
| R | mean radius of the annular chamber |
| $R_o$ | gas constant |
| t | time |
| T | temperature |
| u | velocity component in the axial direction |
| v | velocity component in the tangential direction |

| | |
|---|---|
| $V_w$ | wave propagation velocity |
| x | axial coordinate |
| $x_d$ | detonation length |
| $x_i$ | jet break-up length |
| y | tangential coordinate (= $R\theta$) |
| z | parameter defined in Eq. 11 |
| $\gamma$ | specific heat ratio |
| $\Gamma$ | parameter = $\sqrt{\gamma}\left(\frac{2}{\gamma+1}\right)^{\frac{\gamma+1}{2(\gamma-1)}}$ |
| $\rho$ | spacial density |
| $\theta$ | tangential coordinate |
| $\eta$ | non-dimensional tangential coordinate (= $y/x_d$) |
| $\tau$ | period |
| $\Omega$ | angular velocity |

Subscripts

| | |
|---|---|
| 0 | condition in front of the wave |
| 1 | condition behind the wave |
| b | breakup |
| c | chamber |
| cr | critical |
| d | droplet |
| f | fuel |

| | |
|---|---|
| j | jet |
| o | oxidizer |
| $\ell$ | liquid |
| p | propellant |
| s | condition behind the leading shock |

Superscripts

| | |
|---|---|
| o | condition at absolute zero |
| bar (—) | average value |
| star (*) | non-dimensional quantities |

# I. INTRODUCTION

Randomly distributed small explosions, sometimes described as "popping"[1], often occur in liquid propellant rocket motors. Since the energy released per unit volume near the injector plate is high, these small explosions may often be amplified through detonation-like processes, and finally lead to steep fronted and self sustained pressure waves. This phenomenon is sometimes called "resonant combustion"[2]. The pressure wave resembles the detonation wave in fundamental respects; it propagates supersonically in the circumferential direction at a nearly constant frequency, and the pressure ratio across the wave front has been recorded as high as thirty.

The main objective of recent research in non-linear instability, theoretical as well as experimental (e.g. Refs. 2, 3, 4) is to understand the cause of the finite disturbances and their subsequent amplification. However, should the amplification not be successfully subdued, it becomes imperative that the engine designer know the effects of various design parameters on the final amplitude of the wave. Then the amplitude of the detonation-like wave can at least be reduced to a minimum strength in the design stage. Hence, in this analysis, it is assumed that the non-linear wave is fully developed at its final strength, a two phase detonation wave; the details of its evolution are set aside.

By studying the steady state problem, one can determine the weakening and strengthening effects of various design parameters on the wave amplitude, and thus indicate the proper direction for a stable wave design.

## II. PHYSICAL PICTURE OF ANALYTICAL MODEL

There are several facts which have emerged from experimental studies of the strong wave instability studied here (e.g. Ref. 2); they lead directly to basic assumptions for the analytical model to be described.

First, it is known that the waves rotate at a constant angular velocity, and this is thus taken to be the case in the analysis. A somewhat subtle result of this observation is the condition of periodicity in the fluid properties. For example, since the wave velocity doesn't increase or decrease, the local properties immediately in front of and behind the wave are unchanged with time. In fact, at a given point on the chamber wall, an instrument would always measure the same distribution of pressure (for example) with time, between and across each succeeding wave.

Next, it is observed that the rotating waves are strong near the injector plate, but very weak near the nozzle, and that a wave doesn't "wind up" on itself, that is that even though the strength of the wave varies in the axial direction, the wave angular velocity is the same at each axial location. This is not to say that the whole wave structure is in one plane, for it isn't; it simply means that the weak and strong parts of the wave each travel with the same angular velocity, no matter what the wave shape may be. This is also assumed in the model.

Finally, it is observed that the propellant mass flow rates are not significantly changed from their equilibrium running values when the rotating wave motion occurs, and this is also assumed in the model.

The geometry of the combustion chamber under consideration is shown schematically in Fig. 1. In order to avoid the complexity arising from the radial variations in the governing equations, the analysis is limited to an annular chamber with a thin annulus. However, in a cylindrical chamber, because the wave travels tangentially at a constant angular velocity, it is only near the periphery of the chamber that the wave is strong enough to sustain reaction, and only near the injector plate that significant amounts of propellant droplets exist. Hence, there exists an annulus in which the assumptions made in the present analysis are clearly approximated. Just as in the familiar equilibrium rocket motor performance calculations, viscous forces are taken to be small compared to pressure forces and the heat transfered through the walls is considered to be small compared to the stagnation enthalpy of the gases in the chamber; thus, it is assumed that the chamber walls are frictionless and adiabatic. As a result, between waves, the gas flow is isentropic, and homoenergetic.

A fully developed two phase detonation wave (or waves), rotating at a constant velocity, $V_w (= R\Omega)$, in the negative $\theta$ direction, is considered. It is assumed that this wave front is planar and parallel to the axial direction. It extends an axial distance $x_d$ from the injector plate, where $x_d$

is the distance to which the propellants penetrate between successive waves. Since all propellants are consumed within $x_d$, for $x > x_d$, the wave is a shock rather than a detonation wave. In fact, as will be seen, the detonation branches into two oblique shocks at $x = x_d$. For simplicity, the detonation is treated as a discontinuity, and all reaction is assumed to take place and be completed inside the wave. This assumption is valid as long as the time for droplet breakup and combustion behind the shock part of the detonation wave, is very small compared to the time between waves (or from another viewpoint as long as the wave thickness is small compared to the circumferential distance between waves). It is this condition which sets a limit on the analysis, as will be seen.

Since the wave propagates supersonically, the period of the wave is extremely short (for example the typical wave period of an 11 in. OD chamber is of the order of 470 $\mu$sec). It can be shown[5, 6] for droplets of moderate size (for example 100 microns in diameter) which are typically found in present day rocket motor combustion chambers, that in one wave period the changes in droplet mass, momentum, and temperature are small compared to their initial values. Hence, it may be assumed that the droplets are mechanically and thermally frozen at their injected conditions in one wave period. In addition, the effects of the droplets on the gas motion can be shown to be negligible[5]. Hence,

to good approximation, the two phases near the injector plate may be considered as two independent systems, with phase change occurring only within the detonation wave.

As a result of the side relief offered to the gases immediately behind the detonation wave, in the axial direction, the detonation wave is assumed to be a Chapman-Jouget wave. That is the velocity of the gases leaving the wave, relative to the wave, is sonic, so no more pressure pulses can travel upstream to weaken the wave further.

Finally, it is assumed that the spray is dilute enough that droplet interactions may be ignored, that the gases follow the perfect gas law and are calorically perfect (constant specific heats), and that the energy available through reaction is not changed significantly by changing the mode of reaction. The first two of these assumptions are made for simplicity; the last is justifiable as long as the concentrations of the various species obtained at the end of wave reaction do not vary markedly from the corresponding values which the gaseous products would have in reaction taking place at the design condition. Certainly, as a first approximation, this variation in species concentrations may be neglected from the viewpoint that the propellant mixture ratio and hence the basic energy available is the same; only the mode of reaction is changed during transition from the design condition to the wave running condition. It should be noted that the main effects of different fuels and mixture ratios are introduced through this energy of reaction.

The analytical model described above has emerged as a result of efforts made to simplify the calculations, while still retaining and emphasizing the essential mechanisms. At the nozzle end of the chamber, it resembles a pure acoustic model, because the waves are very weak waves which must travel therefore at essentially acoustic velocities for the mode considered, through gases which are essentially at conditions corresponding to those in the equilibrium running engine. This, plus the fact that all parts of the wave travel at the same angular velocity, explains the success of acoustic theory in predicting wave speeds. At the injector end of the chamber, however, the structure of the model has no relationship whatsoever to an acoustic model. Here, the waves, both detonations and shock waves are strong waves with pressure ratios as high as thirty. The properties of the flow field through which the waves travel are not even closely approximated by the properties in the equilibrium running engine. Typically, the high pressure and temperature immediately downstream of the detonation wave are rapidly decreased by strong expansions from values far above to values below the equilibrium running values. Hence the waves travel through "cold", low pressure regions, compared to the design conditions; even though the velocity of the detonations is nearly the same as that of an acoustic wave in an undisturbed combustion chamber, it is highly supersonic compared to the actual cooler gases through which it passes. Typical pressure distributions, illustrating this point, are shown later.

## III. ANALYSIS

The problem, in view of the rotating wave system, is basically unsteady in terms of a coordinate system fixed to the engine. This complexity can be removed by adopting a coordinate system fixed to the waves and thus rotating at a constant tangential velocity, $V_w$. Such a system is illustrated in Fig. 2, where it is seen that in this case, the waves are stationary and the wall and droplets are moving at a velocity $V_w$. The periodicity found in the original fixed coordinate system is made manifest here by the repetitive nature of the flow picture; e.g., a wave is seen each time a distance L has been traversed in the y direction in Fig. 2, with exactly the same conditions on either side of it as seen on the preceeding wave. Since no frictional forces or wall heat transfer is considered, the motion of the wall presents no computational problems. Because the two phases may be considered as separate systems, the governing equations for the gases can be studied independently of the droplet motion. Finally, since radial variations are neglected, the conservation equations for the gases may be finally reduced in this system to conventional two dimensional steady state equations.

It is seen in Fig. 2, that the effects of the side relief are accounted for by an expansion fan which is centered at the triple point. The strength of the fan must be such as to bring the gas conditions back from their values immediately downstream of the detonation wave to the conditions

which existed immediately upstream of the detonation wave thus satisfying the periodic condition. The strength of the oblique shocks must be such that the pressure must be continuous across, and the velocity vectors must be parallel on either side of, the slip line (the line which separates the flow which goes through the detonation wave from that which passes instead through the shock waves at the triple point). Downstream of the weak wave (characteristic) reflected at the intersection of the last wave of the expansion fan with the wall, the flow is parallel to the wall in the region bounded by the wall and the slip line.

Governing Equations and Method of Solution

As a result of the previously mentioned assumptions, it is easily shown[5] that the specific entropy, and total relative enthalpy which is defined as

$$H = h + \frac{1}{2}(u^2 + v^2 - V_w^2) \tag{1}$$

must be constant along every streamline in the gaseous flow field between any two consecutive waves (see Fig. 2). However, since the detonation wave itself is one dimensional, there is no variation in the specific entropy and total relative enthalpy normal to the streamlines. Consequently, between the waves, the gaseous flow field is isentropic and homoenergetic. Furthermore, in order to satisfy the periodic condition, these two properties must reach the same values in front of the wave in each and every

cycle. Therefore, it is concluded that there should be no net change of the specific entropy and total relative enthalpy of the gases across the detonation wave itself. This in no way violates the Second Law of Thermodynamics, since the entropy of the mixture of gases and droplets does increase across the wave.

The mixture entering the wave consists of burned gases and unburned propellant droplets, while the flow leaving the wave consists only of burned gases. The following non-dimensional quantities are defined:

$$
\begin{aligned}
P_1^* &= P_1/P_o & \rho_1^* &= \rho_1/\rho_o \\
Q^* &= Q/C_p T_o & v_1^* &= v_1/\sqrt{\gamma R_o T_o} \\
V_w^* &= V_w/\sqrt{\gamma R_o T_o} & \rho_d^* &= \rho_d/\rho_o \\
T_1^* &= T_1/T_o & M_o &= v_o/\sqrt{\gamma R_o T_o}
\end{aligned}
\qquad (2)
$$

where the subscripts "o" and "1" refer to conditions upstream and downstream of the wave, respectively, and Q denotes the energy released across the wave per unit mass of propellants; that is

$$Q = h_d - h^o \qquad (3)$$

$\rho_d$ is the spacial density of the propellant droplets. It can be shown[5] that there are eight equations (three from the jump conditions across the two phase detonation wave, two from the condition that the specific entropy and total relative enthalpy of the gaseous phase must be conserved

across the wave, two from the equations of state, and one from the Chapman-Jouguet condition) for the nine parameters associated with the detonation wave, i.e. $P_1^*$, $\rho_1^*$, $T_1^*$, $v_1^*$, $V_w$, $T_o$, $P_o$, $\rho_o$, and $v_o$. These equations may be written as explicit equations for the wave parameters in terms of $M_o$, the local wave Mach number, as follows:

$$T_1^* = B \tag{4a}$$

$$P_1^* = B^{\gamma/(\gamma-1)} \tag{4b}$$

$$\rho_1^* = B^{1/(\gamma-1)} \tag{4c}$$

$$v_1^* = B^{1/2} \tag{4d}$$

$$V_w^* = \frac{\left(\frac{\gamma+1}{\gamma}\right) B^{\gamma/(\gamma-1)} - (M_o^2 + 1/\gamma)}{B^{(\gamma+1)/2(\gamma-1)} - M_o} \tag{4e}$$

$$Q^* = T_c^* = \left(\frac{\gamma+1}{2}\right) B - \left(\frac{\gamma-1}{2}\right)\left\{\frac{\left(\frac{\gamma+1}{\gamma}\right) B^{\gamma/(\gamma-1)} - (M_o^2 + 1/\gamma)}{B^{(\gamma+1)/2(\gamma-1)} - M_o}\right\}^2 \tag{4f}$$

$$\rho_d^* = \frac{\left\{B^{(\gamma+1)/2(\gamma-1)} - M_o\right\}^2}{\left(\frac{\gamma+1}{\gamma}\right) B^{\gamma/(\gamma-1)} - (M_o^2 + 1/\gamma)} \tag{4g}$$

$$\frac{V_w}{a_c} = \frac{\left\{\left(\frac{\gamma+1}{2}\right) B^{\gamma/(\gamma-1)} - (M_o^2 + 1/\gamma)\right\}\left\{B^{(\gamma+1)/2(\gamma-1)} - M_o\right\}^{-1}}{\left\{\left(\frac{\gamma+1}{2}\right) B - \left(\frac{\gamma-1}{2}\right)\left[\frac{\left(\frac{\gamma+1}{\gamma}\right) B^{\gamma/(\gamma-1)} - (M_o^2 + 1/\gamma)}{B^{(\gamma+1)/2(\gamma-1)} - M_o}\right]^2\right\}^{1/2}} \tag{4h}$$

where B depends only on $M_o$ and $\gamma$,

$$B = \frac{2}{(\gamma + 1)} \left[ 1 + \frac{(\gamma - 1)}{2} M_o^2 \right] \tag{5}$$

$T_o$ and $\rho_o$ can be obtained from Eqs. (4f) and (4g) respectively, and $v_o$ and $P_o$ are calculated using the definition of $M_o$ and the equation of state respectively; thus,

$$v_o = M_o \sqrt{\gamma R_o T_o} \tag{6a}$$

$$P_o = \rho_o R_o T_o \tag{6b}$$

It should be noted in Eq. (4f) that $T_c^*$ is the dimensionless chamber temperature, $T_c/T_o$, and that the fact that $Q^* = T_c^*$ is the direct consequence of the fundamental assumption that the energy release is independent of the wave motion. Typical variations of $T_1^*$, $P_1^*$, $V_w^*$, $T_c^*$, $\rho_d^*$, and $V_w/a_c$ with $M_o$, are shown in Figs. 3, 4, and 5, for a representative value of $\gamma = 1.26$. In addition, $P_s^* = P_s/P_o$ and $T_s/T_o$, the pressure and temperature ratios respectively across a shock wave at the same Mach number, $M_o$, are shown for comparison with the corresponding ratios across the two phase detonation wave.

Equations (4) do not afford a complete solution for the parameters of the problem, because, as noted previously, there are so far, only eight relations for nine unknowns. This is seen in Eqs. (4) by the fact that $M_o$ is needed to calculate the remaining parameters. The final necessary relation is found by considering the flow through the nozzle and relating this flow to that from the injector plate.

It is seen, in Fig. 2, that the flow field between the first slip line and the nozzle end of the chamber is very complicated due to the existence of oblique shock waves induced by the detonation wave. However, if these waves become sufficiently weak at the nozzle end, as assumed, the flow through the nozzle may be considered as a mean flow which satisfies the conventional one dimensional flow equations plus two dimensional small disturbances. To the degree of approximation used in this analysis, one may neglect these small disturbances, and employing a control volume which extends from the injector plate to the nozzle entrance and is bounded by the chamber walls, derive conservation equations (for mass, axial momentum, and total relative enthalpy) which relate conditions at the injector plate to the mean flow conditions at the nozzle end. Thus, the difficulties inherent in the irreversible flow region, where many oblique shocks with finite strength exist, can be avoided. As a result, and because the mass rate of propellant flow with waves is unchanged from its design, wave free value, one can relate the average pressure on the injector plate to the design chamber pressure, $P_c$ [5]; that is,

$$\frac{1}{L}\int_0^L P\,dy = P_c\left\{\frac{2\gamma}{(\gamma-1)}\left[1-\frac{\Gamma^2}{2}\frac{A_t}{A_c}^2\right]^{1/\gamma} - \left(\frac{\gamma+1}{\gamma-1}\right)\left[1-\frac{\Gamma^2}{2}\frac{A_t}{A_c}^2\right]\right\} \quad (7)$$

The average pressure on the injector plate may be written as

$$\frac{1}{L}\int_0^L P\,dy = P_o\left\{1 + \frac{x_d}{L} J_2\right\} \tag{8a}$$

$$J_2 = P_1^* \int_0^{\eta_o} \frac{P}{P_1}\, d\eta - \eta_o \tag{8b}$$

where $\eta_o$ ($= y_o/x_d$) is the non-dimensional distance along the injector plate from the wave front to the point where the flow has expanded back to those conditions which exist upstream of the wave front, satisfying the periodic condition. The pressure distribution along the injector plate, $P/P_1$ can be calculated using the method of characteristics[5, 8] since the flow field between consecutive waves is irrotational. It is seen from Fig. 2 that the flow pattern resembles that of half of an under-expanded two-dimensional nozzle with the throat at the Chapman-Jouguet plane and centerline along the wall. The pressure distribution, $P/P_1$, and Mach number, M, along the wall are plotted in Fig. 6. Finally, the pressure distribution can be integrated numerically to obtain the average pressure; curves of $\eta_o$, $\int_0^{\eta_o} (P/P_1)\, d\eta$, and $J_2$ are illustrated in Figs. 3 and 4 for $\gamma = 1.26$. It should be noted that after $P_1$ is obtained, a dimensional pressure distribution along the wall (pressure-space trace) can be obtained easily from Fig. 6. A typical wall pressure trace is shown later (Fig. 8).

From Eqs. (7) and (8) one can show that

$$\frac{P_c}{P_o} = P_c^* = \frac{\left[1 + \frac{x_d}{L} J_2\right]}{\left\{\frac{2\gamma}{(\gamma - 1)}\left[1 - \frac{\Gamma^2}{2}\left(\frac{A_t}{A_c}\right)^2\right]^{1/\gamma} - \left(\frac{\gamma + 1}{\gamma - 1}\right)\left[1 - \frac{\Gamma^2}{2}\left(\frac{A_t}{A_c}\right)^2\right]\right\}} \tag{9}$$

Also, since the total propellant mass flow, which comes from the injectors and passes through the (choked) nozzle, must also enter the detonation wave,

$$A_t \Gamma \frac{P_c}{\sqrt{R_o T_c}} = \rho_d V_w A_c \frac{x_d}{L} \tag{10}$$

Finally, Eqs. (9) and (10) may be combined to give,

$$\frac{\frac{x_d}{L} J_1}{\left(1 + \frac{x_d}{L} J_2\right)} = Z \tag{11}$$

where $J_1$ and Z are defined as follows:

$$J_1 = \rho_d^* T_c^* \frac{V_w}{a_c} \tag{12a}$$

$$Z = \frac{\frac{A_t}{A_c} \frac{\Gamma}{\sqrt{\gamma}}}{\left\{\frac{2\gamma}{(\gamma - 1)}\left[1 - \frac{\Gamma^2}{2}\left(\frac{A_t}{A_c}\right)^2\right]^{1/\gamma} - \left(\frac{\gamma + 1}{\gamma - 1}\right)\left[1 - \frac{\Gamma^2}{2}\left(\frac{A_t}{A_c}\right)^2\right]\right\}} \tag{12b}$$

Using Eqs. (4), one can write J, in terms of $M_o$; this function is shown in Fig. 4 for $\gamma = 1.26$.

Equation (11) is the desired relation to give $M_o$, as a function of $\gamma$, $A_t/A_c$, and $x_d/L$. Since it is not possible to write an explicit functional form for $M_o$, a numerical solution is necessary. A typical plot of a solution to Eq. (11) is shown in Fig. 7, where $x_d/L$ is plotted vs $M_o$ for various constant values of Z for $\gamma = 1.26$. Since $\gamma$ is a given value, Z varies only with the area ratio $A_t/A_c$. The curves are found by setting Z equal to a given value, choosing a value for $M_o$, calculating $J_1$ and $J_2$ (or using Fig. 4) and then calculating $x_d/L$ using Eq. (11). This is done for several values of $M_o$, and repeated for several values of Z, leading to the curves shown in Fig. 7.

Although a typical numerical calculation will be illustrated later, it is worthwhile to point out that at this stage of the calculations, all desired parameters and fluid property variations could be calculated if the following engine design parameter are known:

(1) $A_t/A_c$

(2) $\gamma$

(3) $P_c$

(4) $T_c$ $(a_c)$

(5) $R_o$

(6) $x_d/L$

where, again, $P_c$ and $T_c$ (or $a_c$) are those values associated with the equilibrium running engine, and $R_o$ is the specific gas constant and thus equal to the universal gas constant divided by the molecular weight of the exhaust gases in the equilibrium running engine. The procedure is as follows:

(1) Knowing $A_t/A$ and $\gamma$, calculate Z, using Eq. (12b).

(2) Knowing $x_d/L$ and Z find $M_o$, using Fig. 7. This presupposes a plot such as Fig. 7 for the given $\gamma$.

(3) Knowing $M_o$, calculate B (Eq. (5)) and then $T_1^*$, $P_1^*$, $\rho_1^*$, $v_1^*$, $V_w^*$, $T_c^*$, $\rho_d^*$, and $V_w/a_c$, using Eqs. (4).

(4) Knowing $a_c$ and $T_c$, as well as $V_w/a_c$ and $T_c^*$, calculate $V_w$, and $T_o$.

(5) Calculate $P_c^*$, using Eq. (9), and knowing $P_c$, calculate $P_o$.

(6) Knowing $P_o$, $T_o$, and $R_o$, calculate $\rho_o$, using Eq. (6b).

(7) Knowing $P_o$, $\rho_o$, $T_o$, and $R_o$, as well as $T_1^*$, $P_1^*$, $\rho_1^*$, $v_1^*$, $\rho_d^*$, and $M_o$ calculate $T_1$, $P_1$, $\rho_1$, $v_o$, $v_1$, and $\rho_d$.

The pressure distribution can be obtained by finding $\eta_o$ using Fig. 3, and then calculating $y_o/L = \eta_o \cdot x_d/L$. Then one can use Fig. 6, since $P_1$ is known, to plot P vs y/L up to $y_o/L$, after which $P = P_o$ = constant up to y/L = 1 where a new wave exists. Thus, all quantities of interest can be obtained. It should be noted that knowing both $R_o$ and $a_c$ implies that one knows the fuel-oxidizer mixture ratio.

Calculation of Wave Width, $x_d$

In the previous section, it was shown that in order to obtain a general solution one must know not only the familiar design parameters of a rocket engine, but also $x_d/L$. It is this latter parameter which contains all the parameters associated with the injectors; one must be able to estimate this important parameter for various injector systems.

$x_d$ is taken to be the furthermost penetration distance of spray for the given injection system in the time between successive waves; i.e., it is assumed that no droplets exist beyond $x_d$. For simplicity, it is assumed that the droplet distribution is uniform over $x_d$, that is, that the wave is one dimensional.

In the simple case where droplets are formed at the plane of the injector plate, $x_d$ may be defined as the distance over which droplets move in one wave period, that is,

$$\frac{x_d}{L} = \frac{u_d}{V_w} = \frac{u_d}{a_c} \cdot \frac{a_c}{V_w} \tag{13}$$

where $u_d$ is the average droplet axial velocity, and would be considered to be known. However, it is noted that Eq. (13) generally underestimates the penetration of the spray for those injectors presently in use. Firstly, the spray tends to form at a finite distance from the injector plate, since a finite time is required for the liquid jets to be disintegrated. Secondly,

droplets in the spray are not uniform in size and thus are not uniformly distributed; larger drops penetrate further downstream. Hence, the penetration distance of the actual spray tends to be longer than the penetration distance calculated on the basis of the mean drop size.

There is no known exact theory to predict the penetration distance of the spray during the rotating wave motion. The following analysis is an approximate calculation, wherein the difficulties of the non uniform distribution of droplets in the spray are ignored and a simple expression derived using the equations expressing the conservation of mass and axial momentum of the injected liquid jets. It is assumed that the liquid jets are disintegrated at some distance, $x_i$, from the injector plate, and the jet breakup points are viewed as uniformly distributed sources, from which droplets issue. In the case where the jets are injected into the high speed transverse flow, $x_i$ may be expressed by

$$x_i = u_\ell \, t_b \tag{14}$$

where $u_\ell$ is the velocity of the liquid jet and $t_b$ is the jet breakup time given by[9]

$$t_b \doteq 4 \, \frac{d_j}{|q - q_j|} \sqrt{\frac{\rho_\ell}{\rho}} \tag{15}$$

In Eq. (15), $d_j$ is the jet diameter, $q - q_j$ is the slip velocity between the jet and the surrounding gases, $\rho_\ell$ is the density of the liquid jet, and $\rho$ is the density of the surrounding gases. In the case of impinging jets,

the impingement distance may be used for $x_i$, provided that the impingement distance is less than the length calculated using Eq. (14).

By using the conditions that the mass and axial momentum of droplets after breakup must be equal to the corresponding properties of the liquid jets coming into the point sources, a simple expression for $x_d/L$ can be derived[5];

$$\frac{x_d}{L} = 2\frac{x_i}{L} + \frac{u_j}{V_w} \tag{16}$$

where $u_j$ is the mean jet velocity. In the case where bipropellants are used, then,

$$u_j = \frac{1}{(1+f)} u_f + \frac{f}{(1+f)} u_o \tag{17}$$

where f is the oxidizer to fuel ratio, and $u_f$ and $u_o$ are the axial velocity components of the fuel and oxidizer, respectively. Due to the difficulty in assessing the effects of the rotating wave motion on the jet breakup, $x_i$ is approximated here by the predicted wave free jet breakup distance for the given injection system.

Example Calculation; Comparison with Experiment

A series of experiments on detonation-like wave motions were conducted at JPL[11-14] for various design conditions which are listed in Table I. In order to test the validity of the present analysis these design conditions were used to calculate various wave and flow properties for

comparison with experimental results. A typical calculation is presented here to illustrate the method of solution in detail. It should be noted that all the design conditions and experimental data presented in Table I are for cylindrical chambers; as mentioned previously, however, there is an annulus in the cylindrical chambers, where the assumptions used here are met. Only data from those transducers located in this annulus, i.e. near the corner made by the injector plate and the chamber wall, are used for comparison. Some are located on the injector plate and some on the wall.

For the calculation to be made now, the design parameters of Ref. 11 (Table I) are used. In addition, $\gamma$ is chosen to be 1.26. Thus, $A_t/A_c = 1/2$, $a_c = 3530$ ft/sec, $P_c = 300$ psia, $x_i = 0.75$ in., $L = 34.54$ in. (for one wave), $f = 2.8$, $q_f = 148$ ft/sec, $q_o = 86$ ft/sec, $\theta_f = 28^o\ 18'$ and $\theta_o = 15^o\ 42'$. Here $q_f$ and $q_o$ are the velocities of the fuel and oxidizer liquid injection jets respectively, and $\theta_f$ and $\theta_o$ are the corresponding angles made by these jets with respect to the axial direction. The injectors are of the impinging type and so $x_i$ is taken to be the axial impingement distance from the injector plate.

From Eq. (12b), z is calculated to be 0.2796. Next from Eq. (17), $u_j$ is calculated to be 93.6 ft/sec. Then, from Eq. (16),

$$x_d/L = 0.0432 + 0.0265(a_c/V_w) \tag{18}$$

where $V_w/a_c$ is given in terms of $M_o$ by Eq. (4h). If Eq. (18) is plotted on Fig. 7 (dashed line) it is found to intersect the $z = 0.2796$ curve at $M_o = 2.73$, and $x_d/L = 0.0575$. With this value of $M_o$, $V_w/a_c = 1.847$ (from Fig. 3 or Eq. (4h)), $P_1^* = 14.74$ (from Fig. 5 or Eq. (4b)), $J_2 = 18.1$ (from Fig. 4, defined by Eq. (8b)), and $P_c^* = 1.94$ (Eq. (9)). Other desired parameters such as $T_1^*$, etc., could be found in the same way by using Figs. 3 and 4 or Eqs. (4). Since $P_c = 300$ psia, then $P_o = P_c/P_c^* = 155$ psia, and $P_1 = P_o/P_1^* = 2280$ psia. Since $a_c = 3530$ ft/sec, $V_w = a_c (V_w/a_c)$ = 6520 ft/sec. The calculated and experimental results are both shown in Table II for this and other cases. It is seen that the analytical results compare quite favorably with the experimental data, especially in the case of Ref. 11.

After $P_1$ is obtained, the dimensional pressure distribution along the injector plate can be obtained easily from Fig. 4, after determining $\eta_o$ from Fig. 3. In this case, for $M_o = 2.73$, $\eta_o = 4.63$, so $y_o/L = \eta_o (x_d/L)$ = 0.266. For $y > y_o$, of course, the pressure is constant at $P_o$. In Fig. 8, the calculated pressure distribution is shown and compared with an experimentally measured pressure trace obtained from Ref. 11. The agreement is seen to be excellent.

## IV. EFFECT OF DESIGN CHANGES ON WAVE STRENGTH

It is of interest to use the results given by the preceding analysis to predict the effects of various design parameters on the wave strength which is characterized here by the detonation wave pressure ratio, $P_1^* = P_1/P_o$. In each case, the effects are illustrated in the form of a plot of $P_1^*$ versus the design parameter in question, other parameters being held constant at those values listed under Ref. 11 in Table I and used in the example problem, except where noted.

### 1. Contraction Ratio, $A_t/A_c$

A plot of $P_1^*$ vs $A_t/A_c$ is shown in Fig. 9, for $\gamma = 1.26$ and for $x_d/L$ constant. A point may be calculated by choosing an $M_o$, and finding the corresponding $P_1^*$, $J_1$, $J_2$, and $V_w/a_c$ points from Figs. 3, 4, and 5. $x_d/L$ is here chosen to be the value calculated in the example calculations, $x_d/L = 0.0575$. With $x_d/L$, $J_1$, and $J_2$ known, z may be calculated using Eq. (11), and the corresponding $A_t/A_c$ value may be found using Eq. (12b). By choosing several values of the parameter $M_o$, the $P_1^*$ and corresponding $A_t/A_c$ values can be calculated and plotted as shown in Fig. 9. In addition, a few points with $x_d/L$ varying as in Eq. (18) were calculated and are shown for comparison; this variation has a minimal effect.

It is seen that as $A_t/A_c$ increases, the pressure ratio, $P_1^*$, increases; the wave becomes stronger. Conversely, decreasing the contraction ratio has a stabilizing effect (wave becomes weaker). It can also be shown,

using Eqs. (4) that the wave speed increases or decreases the same as $P_1^*$. This result is also found experimentally[10].

2. Chamber Radius, $R = L/2\pi$

For a given $x_d$, $x_d/L$ increases as R decreases, and it is seen in Fig. 10 that for other design parameters being held constant (most importantly a constant contraction ratio), decreasing R results in decreasing $P_1^*$. Thus as engine size increases, for geometrically similar engines, the wave strength increases. Again, $V_w$ varies in the same manner as $P_1^*$.

The curve of $P_1^*$ versus R can be calculated as follows. For $A_t/A_c = 1/2$ and $\gamma = 1.26$, $z = 0.2796$. Then by choosing various values of $M_o$, and finding the corresponding $P_1^*$ and $x_d/L$ values from Figs. 5 and 7, one can calculate $L = x_d/(x_d/L) = 2\pi R$ for each $M_o$ and thus for each $P_1^*$. $x_d$ was chosen to be the value found in the example calculation, $x_d = 0.0575 \cdot 11 \cdot \pi = 1.99$ in. (Note that Eq. (11) may be used rather than Fig. 7, with $J_1$ and $J_2$ given in Fig. 4.)

3. Droplet Injection Velocity, $u_j$

In this case, the mass rate of flow of propellants is held constant and $u_j$ is varied by changing the injector areas. In addition, impinging jets are assumed, so Eq. (16) is employed. It is seen in Fig. 11 that

as $u_j$ increases (which corresponds to an increase in $x_d$), $P_1^*$ decreases. The effect of increasing the jet velocity is to weaken the detonation wave. $V_w$ varies in the same way as $P_1^*$.

The computations for Fig. 11 are performed as follows. Equation (16) is rearranged to give,

$$u_j = \left(\frac{x_d}{L} - \frac{2x_i}{L}\right) \frac{V_w}{a_c} \cdot a_c$$

For these calculations, $2x_i/L = 0.0432$ and $a_c = 3530$ ft/sec, the values from the example problem. Again, for $A_t/A_c = 1/2$ and $\gamma = 1.26$, $z = 0.2796$. The points are found by choosing values of $M_o$, finding corresponding values of $V_w/a_c$, $x_d/L$, and $P_1^*$ from Figs. 3, 5, and 7, and calculating the corresponding value of $u_j$ from the above equation.

4. Chamber Pressure, $P_c$, and Chamber Speed of Sound, $a_c$

$P_c$ and $a_c$ are considered simultaneously since they are intimately related by the mass flow relation, i.e., $\dot{m}_p \propto P_c/a_c$. In the first case considered here $\dot{m}_p$ is held constant. In Fig. 12, $P_1^*$ is plotted vs $a_c$ for the case of impinging jets, so Eq. (16) is used for $x_d/L$; since $\dot{m}_p$ is constant, $P_c$ varies also. $P_c$ is plotted vs $a_c$ in Fig. 13. This case corresponds to changing propellants or mixture ratios, holding other parameters constant. It is seen that as $a_c$ increases, $P_1^*$ and $P_c$ both increase. Moreover, since $P_c^*$, plotted also in Fig. 12, remains

relatively constant, then $P_o$ increases as $P_c$ increases. Thus, not only the pressure ratio, $P_1^*$, but also the pressure levels (i.e., $P_o$ and $P_1$) increase. Since $V_w/a_c$ increases or decreases when $P_1^*$ increases or decreases, and $P_1^*$ increases as $a_c$ increases, $V_w$ increases even more rapidly than $a_c$ (i.e., $V_w = (V_w/a_c)\, a_c$).

The curves in Figs. 12 and 13 may be computed as follows. From Eqs. (16), (9), (12b), and (10), one can show that

$$a_c = \frac{u_j}{\left(\frac{x_d}{L} - \frac{2x_i}{L}\right)} \cdot \frac{a_c}{V_w}$$

$$P_c^* = \left(1 + \frac{x_d}{L} J_2\right) z \frac{\sqrt{\gamma}}{r} \frac{A_c}{A_t}$$

$$P_c = \frac{\dot{m}_p}{A_c} \frac{A_c}{A_t} \cdot \frac{a_c}{r\sqrt{\gamma}}$$

For these calculations, the values employed in the example calculations were used. Thus,

$$A_t/A_c = 1/2 \qquad \gamma = 1.26 \qquad z = 0.2796$$

$$u_j = 93.6 \text{ ft/sec} \qquad 2x_i/L = 0.0432 \qquad \dot{m}_p/A_c = 1 \text{ lbm/in.}^2 \text{ sec}$$

where the value of $\dot{m}_p/A_c$ is that corresponding to the other parameters in the example calculation as seen in Column 1 of Table I. As in previous

calculations, various values of the parameter $M_o$ are chosen and corresponding values of $x_d/L$, $V_w/a_c$, $J_2$, and $P_1^*$ are found from Figs. 7, 3, 4, and 5 respectively. Then the above equations may be used to calculate the corresponding values of $a_c$, $P_c^*$, and $P_c$.

It should be noted that if an injection system where $x_d/L$ is a constant were considered, for this case where $\dot{m}_p$ is held constant, then from Fig. 7 it is seen that since z is also a constant, $M_o$ would be a constant. Hence, from Fig. 5, $P_1^*$ would also have a constant value as $a_c$ and $P_c$ increased. However, since $P_c^*$ (see Eqs. (9) and (12b)) would also remain constant, $P_o$ would increase as $P_c$ increased. Likewise $P_1 = P_o \cdot P_1^*$ would increase as $P_c$. The result would be a case where the pressure levels increased in such a way that the pressure ratio, $P_1^*$, remained constant. In addition since from Fig. 3, $V_w/a_c$ would have a single value (for one value of $M_o$), $V_w$ would vary directly as $a_c$.

The second case to be considered here is that where $a_c$ is held constant and $P_c$ is varied, so that the propellant mass flow rate, $\dot{m}_p$, varies. However, $u_j$ is held constant so that the $\dot{m}_p$ variation is due entirely to variations in the cross sectional area of the injectors. Again impinging jets are assumed so that Eq. (16), holds, written again here as

$$u_j = \left(\frac{x_d}{L} - \frac{2x_i}{L}\right)\frac{V_w}{a_c} \cdot a_c$$

Now, $x_i/L$, $u_j$, and $a_c$ are constants, and it is seen from Figs. 7 and 3 that since z is a constant, $x_d/L$ and $V_w/a_c$ depend only on $M_o$. That is, the above equation could be written with $M_o$ as the only unknown parameter and thus it could be used to calculate the value of $M_o$ for the case in question. That is, $M_o$ is a constant. Hence, from Fig. 5, $P_1^*$ is constant and the plot of $P_1^*$ vs $P_c$ would be simply a straight line, $P_1^*$ = constant. Thus, from Figs. 3 and 7, or Eqs. (4), and from Eq. (9), $V_w/a_c$, $x_d/L$, and $P_c^*$ have constant values. Then, as $P_c$ increases;, with $a_c$ constant, $P_o = P_c/P_c^*$ increases and $P_1 = P_1^* \cdot P_o$ increases; the pressure levels increase such that the pressure ratio remains unchanged. The wave speed, $V_w = (V_w/a_c)\, a_c$ remains unchanged.

5. Droplet Penetration Distance, $x_d$

The droplet penetration distance is a parameter controlled by the type of injector system employed and is thus indirectly a design parameter. In Fig. 10, the graph of $P_1^*$ vs $x_d$ indicates that as $x_d$ increases, the wave strength decreases. In this case it can also be shown easily, from Figs. 7 and 3 that as $x_d$ increases, $V_w$ decreases.

Calculations for the curve of $P_1^*$ vs $x_d$ in Fig. 10 are made as follows. $A_t/A_c = 1/2$ and $\gamma = 1.26$ are assumed so $z = 0.2796$. Then, various values of $M_o$ are chosen and corresponding values of $P_1^*$ and $x_d/L$ are found from Figs. 5 and 7. Finally $x_d = (x_d/L)\, L$ and L is chosen to be the value in the example calculation, $L = 11 \cdot \pi = 34.54$ in.

## V. LIMIT OF THE ANALYSIS

In Ref. 10, it is shown experimentally that an increase in drop size has a stabilizing effect, i.e. that the wave strength is decreased. On the basis of the present analysi s, this effect may be explained by noting that the larger droplets tend to penetrate farther downstream, leading to a larger $x_d$, and hence a smaller $P_1^*$. However, the drop size effect is not formally incorporated into the present theory due to the fundamental assumption that the wave is treated as a discontinuity. Now it has been shown[15], that the reaction zone length in a two-phase detonation wave increases with drop size; hence losses due to lateral expansion occurring inside the reaction zone must become important at some point as the drop size is increased, and the thin wave assumption breaks down. Evidently the theory cannot be valid for droplets of all sizes. Although a detailed analysis of the structure of the reaction zone is not available, it is possible to set at least a rough limit on the drop sizes for which the analysis is valid.

The structure of a spray detonation has been observed experiementally[16]. The study indicates that much of the mass transfer from the droplet is associated with a local explosion during droplet breakup. Hence, it is believed that a great portion of the energy released from the droplet may be associated with a blast wave initiating from the explosion site,

and that the interaction between the blast wave and the leading shock part of the detonation wave, may be mainly responsible for the energy transmission. On the basis of this observation, a simple criterion for the existence of a strong thin wave may be formulated. That is, the time required for a sound wave initiating at the explosion site of the disintegrating drop to propagate upstream to the leading shock must be equal to or less than the time required for the same wave to propagate laterally the distance to which the detonation extends. If conditions immediately behind the shock are used to estimate the sound velocity and known expressions for droplet breakup times[17] are used, this criterion finally leads to calculation of the critical drop diameter for a wave of given strength. A detailed derivation is given in Ref. (5); the resulting critical drop diameter is,

$$d_{cr} = \frac{1}{4}\left[\frac{x_d}{L} A_c \frac{\dot{m}_p}{\rho_p}\right]^{1/2} J_3 \qquad (19a)$$

$$J_3 = \left(1 - M_s\right)\left(1 - \frac{v_s^*}{v_w^*}\right)\left[\frac{T_c^{*1/2}}{v_w^*} \frac{\rho_s^*}{\rho_d^*}\right]^{1/2} \qquad (19b)$$

where the subscript s refers to conditions behind the leading shock and $\dot{m}_p/\rho_p$ is the average volumetric flow rate, $\rho_p$ being the average liquid density[5]. $J_3$ is plotted in Fig. (14) for $\gamma = 1.26$. If $\bar{d}$ is the average drop diameter calculated for the given injection system, then Eq. (19a)

leads to the following conclusions:

(1) The strong wave analysis is valid if $d \leq d_{cr}$.

(2) Weak waves, which may not be properly described as detonations, are likely to occur if $\bar{d} > d_{cr}$.

There are experimentally correlated equations to calculate $\bar{d}$ for different types of atomization[18]. For the case of impinging jets, for example, the following equation may be used to calculate the mass median drop diameter[19]

$$\bar{d} = 6.92 \times 10^4 \left[ \frac{d_f^{0.27} \, d_o^{0.023}}{q_f^{0.74} \, q_o^{0.33}} \right] \tag{20}$$

where the diameters of the fuel and oxidizer injectors, $d_f$ and $d_o$ respectively, are in inches and the jet velocities of the fuel and oxidizer, $q_f$ and $q_o$ respectively, are in ft/sec.

If $\bar{d}$ and $d_{cr}$ are calculated for each of the experimental conditions covered in Table I, it can be shown[5] that only in the case of Ref. 11 is $\bar{d}$ less than $d_{cr}$; it is for this case also that the comparison between theory and experiment is most satisfactory. Evidently the waves in the remaining cases (see Table II) do not satisfy a strong wave criterion.

# VI. CONCLUSIONS

This study is concerned with tangential mode detonation-like phenomena in liquid propellant rocket motors. It is found that the amplitude of the wave, measured by the pressure ratio across it ($p_1^*$), may be reduced by reducing the contraction ratio ($A_t/A_c$), and chamber diameter, and by increasing the spray penetration distance during the wave running condition ($x_d$). Expressions for $x_d$ are provided. It is found that $x_d$ increases as the jet velocity and projected jet breakup distance increase. In general, the variation of the wave speed follows the same trends as the wave pressure ratio.

For a given contraction ratio, the effects of the chamber speed of sound and chamber pressure depend on the type of injector system used, and upon the propellant mass flow rate. In general, as $a_c$ and $p_c$ increase the pressures immediately upstream and downstream of the wave, and the wave velocity, increase. In some cases, the pressure ratio across the wave also increase, and in others it remains unchanged.

Finally, the limit of the strong wave analysis due to the finite drop size is discussed. A critical drop size, above which a strong wave probably cannot occur is derived, to set a lower limit of validity on the strong wave analysis.

| References | 11 | 12 | 13 | 14 |
|---|---|---|---|---|
| Propellants | SFNA + Corporal fuel | $N_2O_4$ + 50% $N_2H_4$ 50% UDMH | $N_2O_4$ + $N_2H_4$ | $N_2O_4$ + 50% $N_2H_4$ 50% UDMH |
| $a_c$ (ft/sec) | 3530 | 4070 | 4120 | 3850 |
| Chamber radius (inch) (cylind. cham.) | 5.5 | 5.5 | 5.5 | 9 |
| $q_f$ (ft/sec) | 138 | 85 | 75 | 86 |
| $q_o$ (ft/sec) | 86 | 52 | 65.5 | 58 |
| $x_i$ (inch) | 0.75 | 0.982 | 0.982 | 0.625 |
| $\theta_f$ | $28^o18'$ | $22^o30'$ | $22^o30'$ | $35^o36'$ |
| $\theta_o$ | $15^o42'$ | $22^o30'$ | $22^o30'$ | $24^o24'$ |
| $f = \frac{m_o}{m_f}$ | 2.8 | 1.32 | 1.18 | 2.11 |
| $m_p/A_c$ ($lb_m/in^2 sec$) | 1 | 0.875 | 0.88 | 0.31 |
| $p_c$ (psia) | 300 | 320.5 | 273.5 | 100 |
| $d_f$ (inch) | 0.0986 | 0.173 | 0.173 | 0.101 |
| $d_o$ (inch) | 0.173 | 0.173 | 0.173 | 0.142 |
| $(sp.\ grav.)_f$ | 1.073 | 0.892 | 1.01 | 0.892 |
| $(sp.\ grav.)_o$ | 1.55 | 1.45 | 1.45 | 1.45 |

Table I. Geometric and operating parameters of the equilibrium running chamber $\left(\frac{A_t}{A_c} = \frac{1}{2}\right)$.

| | Run | $V_w$ ($ft^2/sec$) | $P_1$ (psia) | $P_0$ (psia) | $\frac{P_1}{P_0}$ | $\tau$ |
|---|---|---|---|---|---|---|
| Experiments (Ref. 11) | B 958 | 6116 | 2392 | 126 | 18.98 | 473 |
| | B 956 | 6103 | 2351 | 121 | 19.43 | 474 |
| | B 955 | 6116 | 2469 | 272 | 9.08 | 473 |
| | Aver. | 6113 | 2404 | 176 | 13.65 | 473 |
| Analysis | | 6520 | 2280 | 155 | 14.74 | 442 |
| Experiments (Ref. 12) | B 979 | 6775 | 882 | 187 | 4.72 | 427 |
| | B 979 | 6775 | 1189 | 185 | 6.43 | 427 |
| | Aver. | 6775 | 1036 | 186 | 5.57 | 427 |
| Analysis | | 7600 | 2145 | 151 | 14.2 | 378 |
| Experiments (Ref. 13) | B 999 | 6871 | 1145 | 127 | 9.02 | 421 |
| | B1000 | 6954 | 998 | 138 | 7.23 | 416 |
| | Aver. | 6928 | 1073 | 133 | 8.08 | 419 |
| Analysis | | 7700 | 1830 | 129 | 14.2 | 374 |
| Experiments (Ref. 14) | B1090 | 6825 | 877 | 37 | 23.7 | 692 |
| | B1093 | 6855 | 891 | 49 | 18.18 | 689 |
| | B1097 | 6885 | 455 | 36 | 12.64 | 686 |
| | Aver. | 6855 | 741 | 40.7 | 18.2 | 689 |
| Analysis | | 7460 | 1320 | 44.6 | 29.6 | 630 |

Table II. Comparison of experimental and analytical results.

## REFERENCES


1. Clayton, R. M., "Experimental Observations Relating to Inception of Liquid Rocket Engine Popping and Resonant Combustion to the Stagnation Dynamics of Injection Impingement," JPL TR 32-1479, Dec. 15, 1970.

2. Clayton, R. M., Rogero, R. S., and Sotter, J. G., "An Experimental Description of Destructive Liquid Resonant Combustion," AIAA J., Vol. 6, No. 7, July 1968, pp. 1252-1260.

3. Crocco, L. and Michell, C. E., "Non-linear Periodic Oscillation in Rocket Motors with Distributed Combustion," Combustion Science and Technology, Vol. 1, 1969, pp. 147-169.

4. Berstein, S. Z., "Non-linear Combustion Instabilities in Liquid Propellant Rocket Engines," JPL TR 32-111, September 15, 1967.

5. Shen, I-wu, "Theoretical Analysis of a Rotating Two Phase Detonation in a Liquid Propellant Rocket Motor," Ph. D. Thesis, The University of Michigan, 1971. Also see Sen, I-wu and Adamson, T. C., Jr., "Theoretical Analysis of a Rotating Two Phase Detonation in Liquid Rocket Motors," Astronautica Acta, Vol. 17, 1972, pp. 715-728.

6. Priem, R. J. and Heidman, M. F., "Propellant Vaporation as a Design Criterion for Rocket-Engine Combustion Chambers," NASA TR R-67, 1968.

7. Sotter, J., Woodward, J. W., and Clayton, R. M., "Injector Response to Strong, High Frequency Pressure Oscillations," J. of Spacecraft and Rockets, Vol. 6, No. 4, April 1969, pp. 504-506.

8. Shamus, H. and Sesshore, F. L., "Design Data for Graphical Construction of Two Dimensional Sharp-Edge-Throat Supersonic Nozzle," NACA RM E8J12, Dec. 1948.

9. Clark, B. J., "Breakup of a Liquid Jet in a Transverse Flow of Gas," NASA TND 2424.

10. Netzer, D. W. and Osborn, J. R., "Investigation of Combustion Characteristics of a Bi-phase Rocket," Purdue University, TM 68-2, 1968.

11. Clayton, R. M. and Rogero, R. S., "Experimental Measurements on a Rotating Detonation-Like Wave Observed During Liquid Rocket Resonant Combustion," JPL TR 32-788, Aug. 15, 1965.

12. Clayton, R. M., "Resonant Combustion," JPL Space Programs Summary 37-36, Vol. IV, Dec. 31, 1965.

13. Clayton, R. M., "Resonant Combustion," JPL Space Programs Summary, 37-43, Vol. IV, Feb. 28, 1967.

14. Clayton, R. M., "Resonant Combustion," JPL Space Programs Summary 37-49, Vol. III, Feb. 29, 1969.

15. Dabora, E. K., Ragland, K.W., and Nicholls, J. A., "Drop-Size Effects in Spray Detonation," 12th Symposium (International) on Combustion, 1969, Combustion Institute, Pittsburgh, pp. 19-25.

16. Ragland, K. W., Dabora, E. K., and Nicholls, J. A., "Observed Structure of Spray Detonation," Physics of Fluids, Vol. 11, No. 11, 1968, pp. 2377-2388.

17. Dabora, E. K., Ragland, K. W., Ranger, A. A., and Nicholls, J. A., "Two Phase Detonation and Drop Shattering Studies," NASA Report CR 72225, 1967.

18. Fraser, R. P., "Liquid Fuel Atomization." Sixth Symposium, (International) on Combustion, Reinhold Publishing Corp. 1956, pp. 687-700.

19. Dickerson, R. D., Tate, K., and Barsic, N., "Correlation of Spray Injector Parameters with Rocket Engine Performance," AFRPL TR 68-147, June 1968.

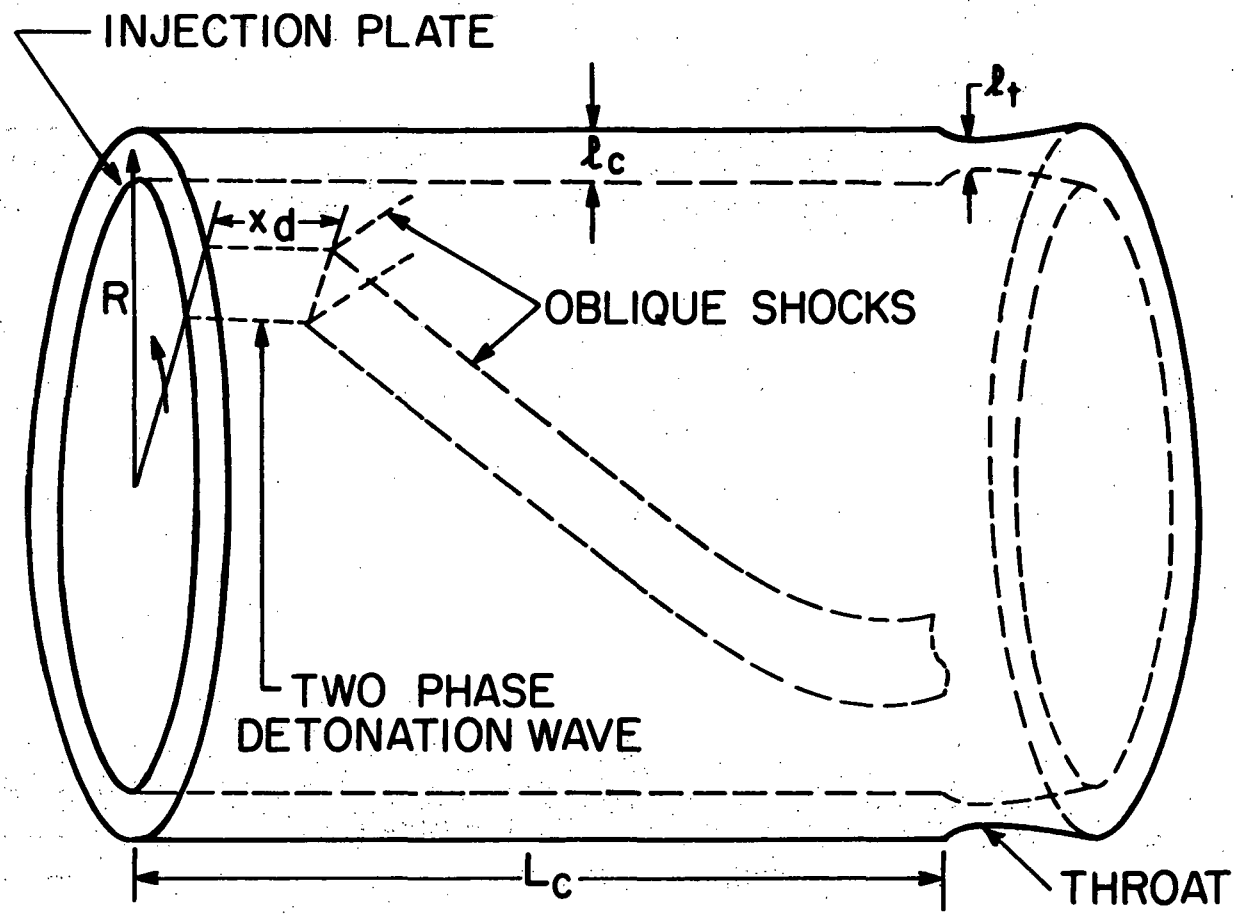


Fig. 1. Geometry of the Annular Chamber.

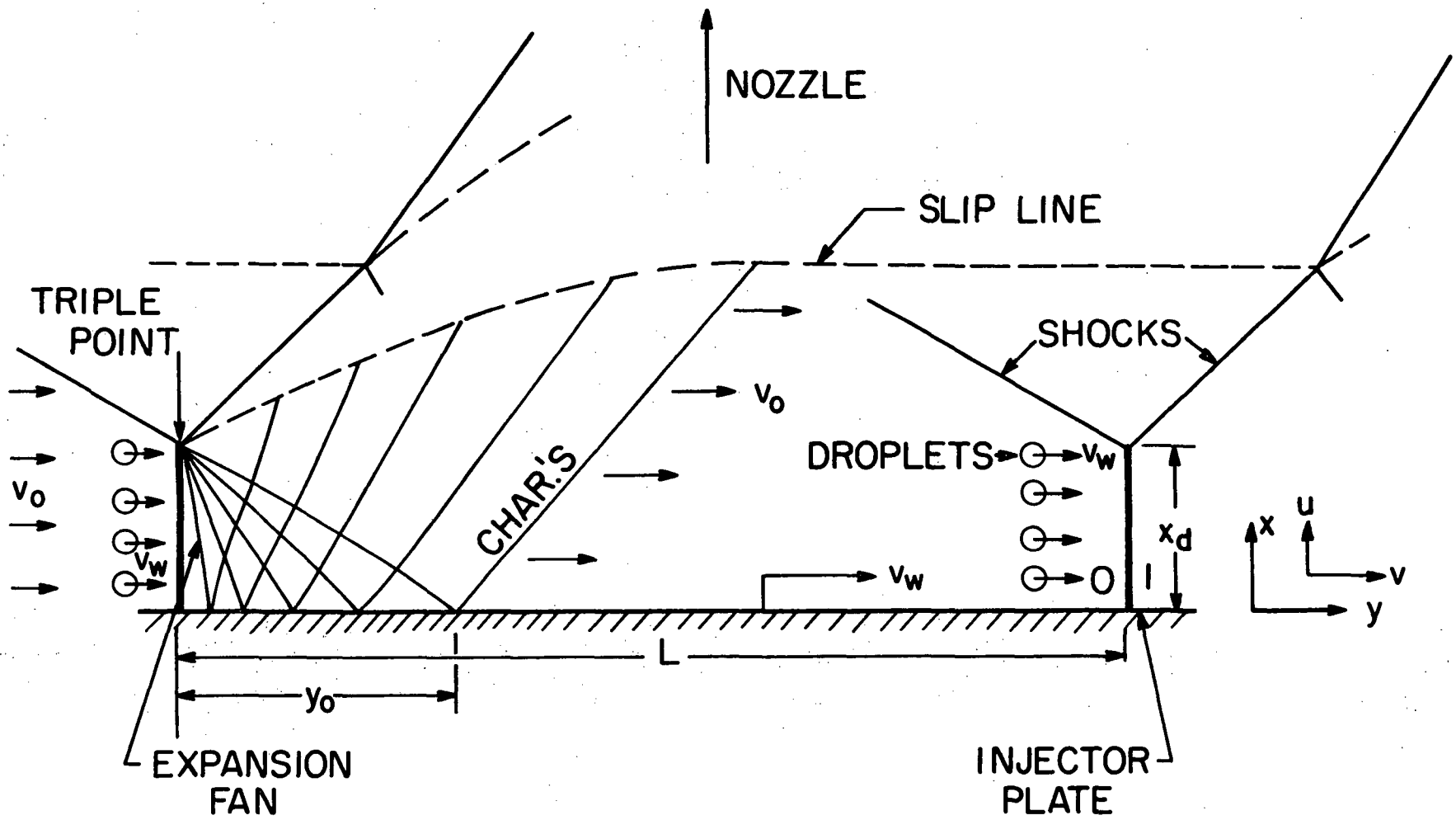


Fig. 2. Flow Pattern Between Two Consecutive Waves in the Wave-Fixed Coordinate System.

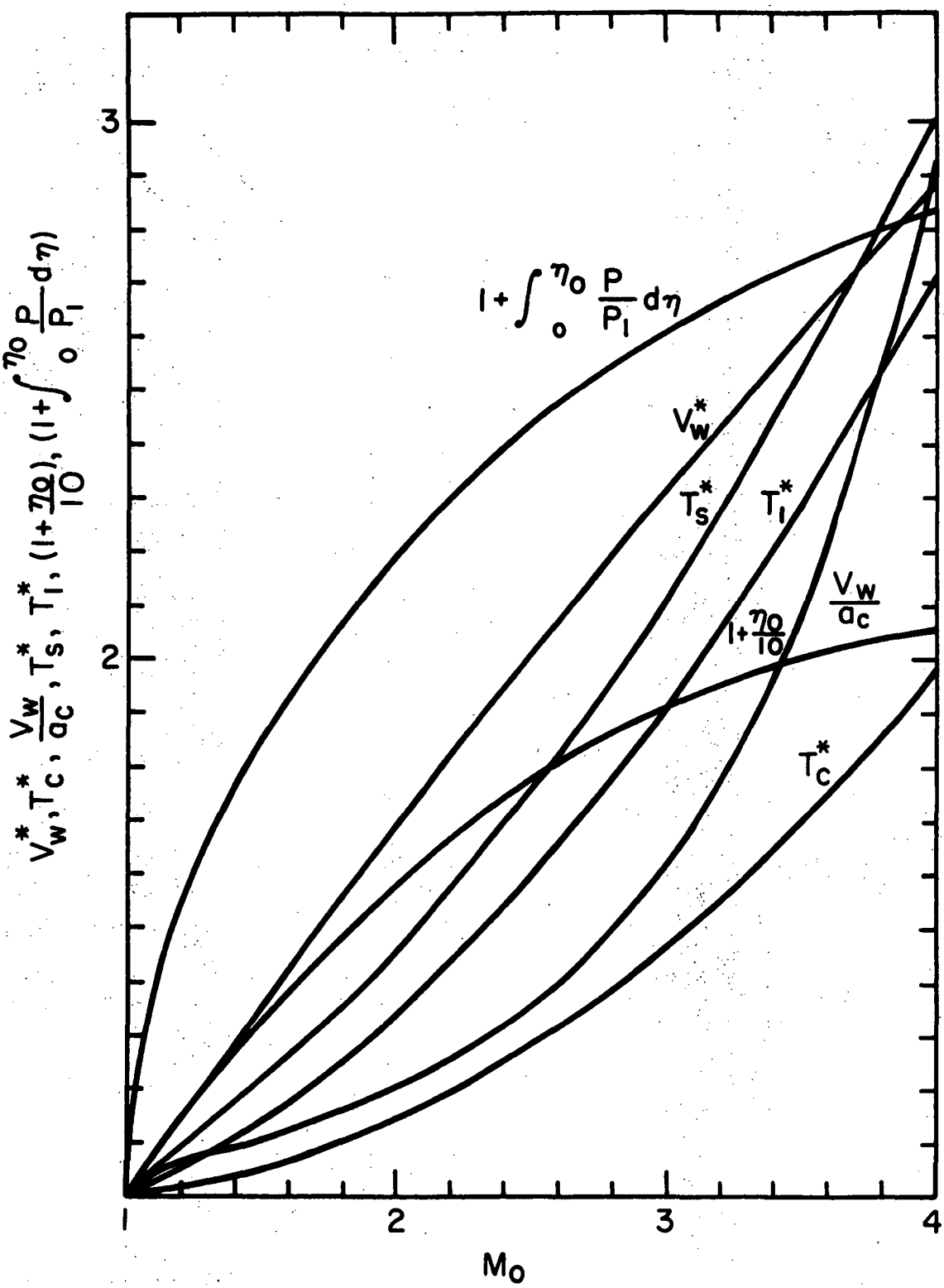


Fig. 3. $V_w^*$, $T_c^*$ (= $Q^*$), $T_s^*$, $T_1^*$ $(1 + \eta_o/10)$, $V_w/a_c$, and $1 + \int_0^{\eta_o} (P/P_1)\, d\eta$ versus $M_o$ for $\gamma = 1.26$.

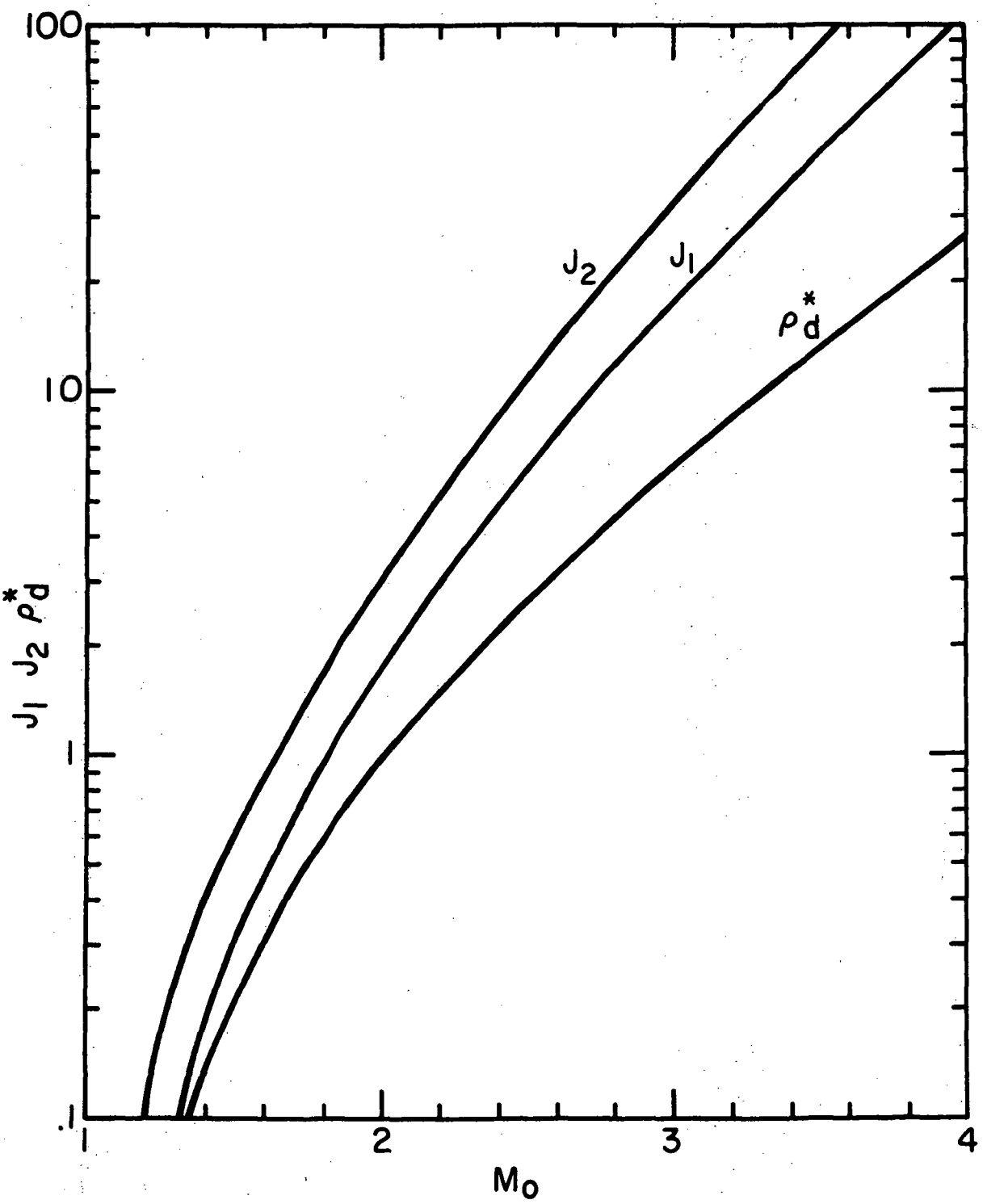


Fig. 4. $\rho_d^*$, $J_1$, and $J_2$ versus $M_o$ for $\gamma = 1.26$.

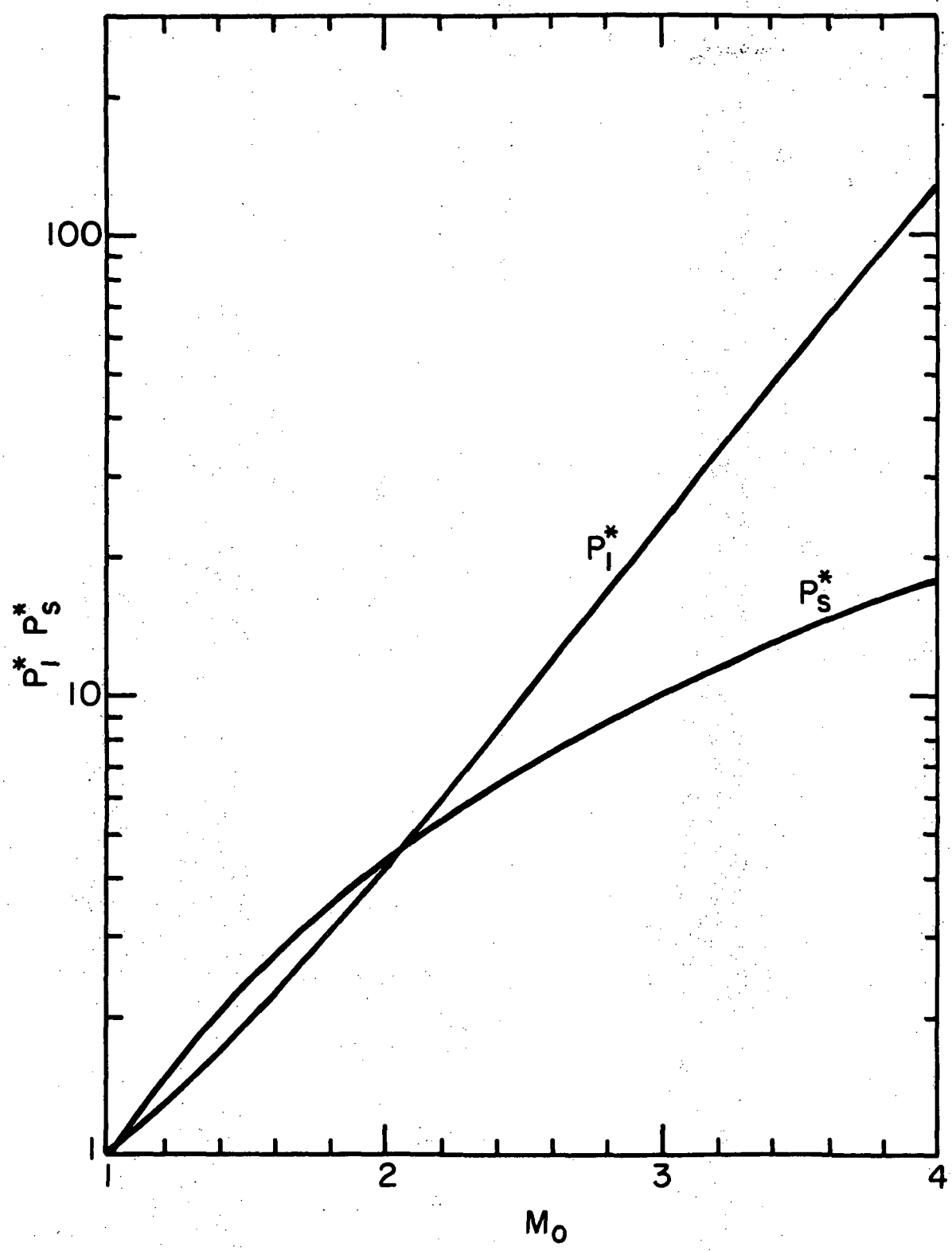


Fig. 5. $P_1^*$ and $P_s^*$ versus $M_o$ for $\gamma = 1.26$.

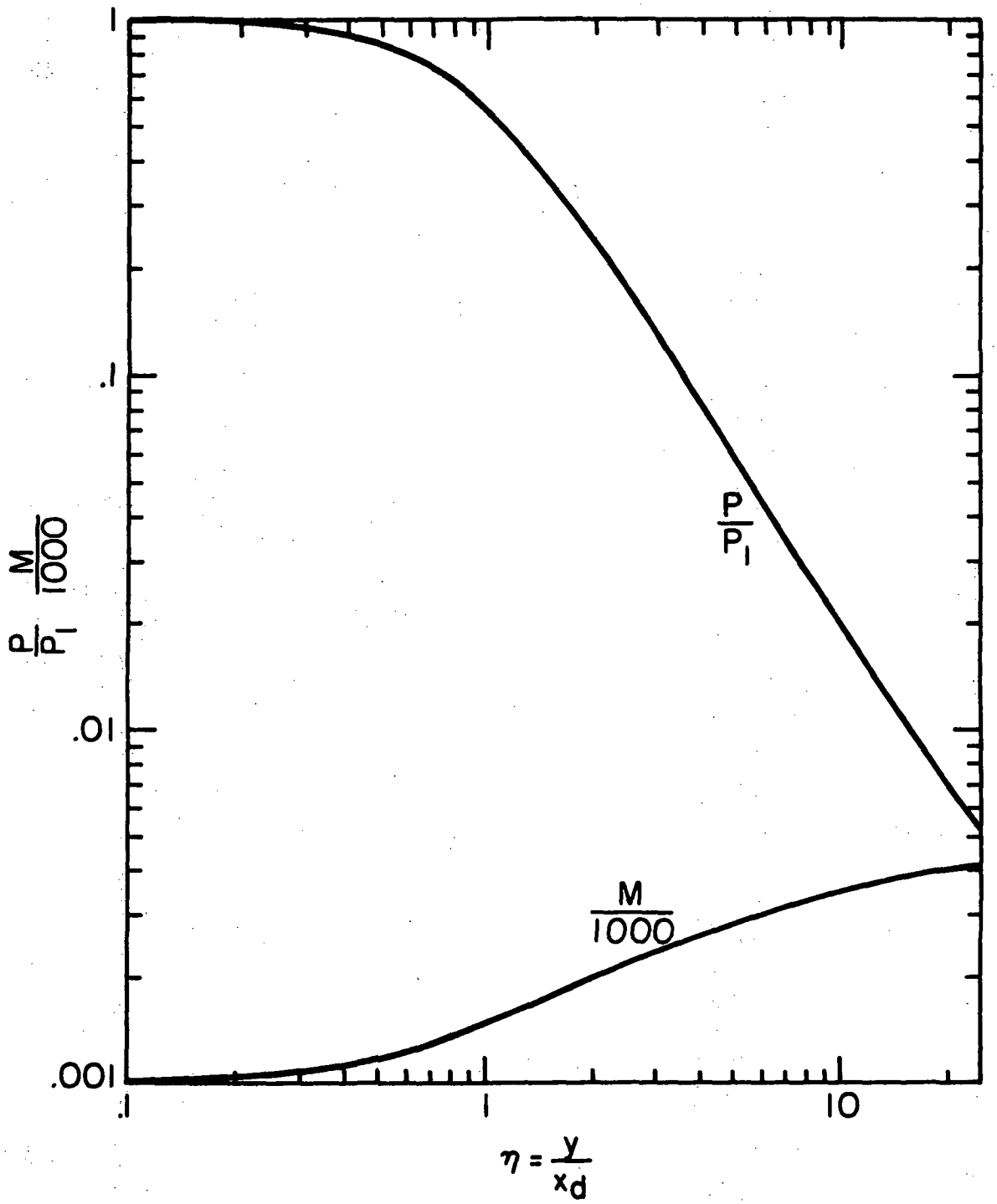


Fig. 6. Distribution of $P/P_1$ and M Along Injector Plate.

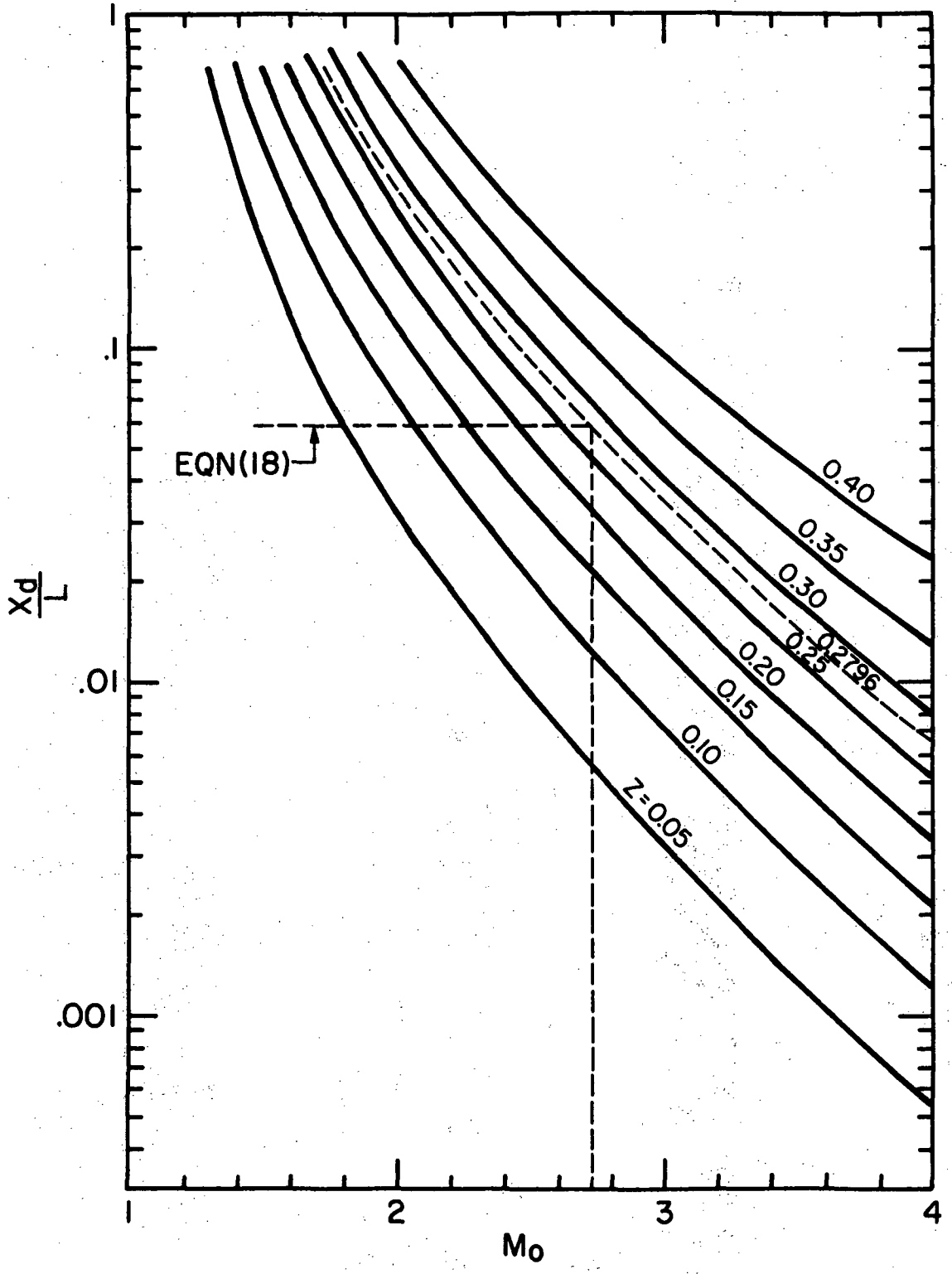


Fig. 7. $x_d/L$ versus $M_o$ for given values of z and $\gamma = 1.26$. Dotted Lines Show Intersection of Eq. (18) with Curve for z = 0.2796, giving $M_o = 2.73$ for Example Calculation.

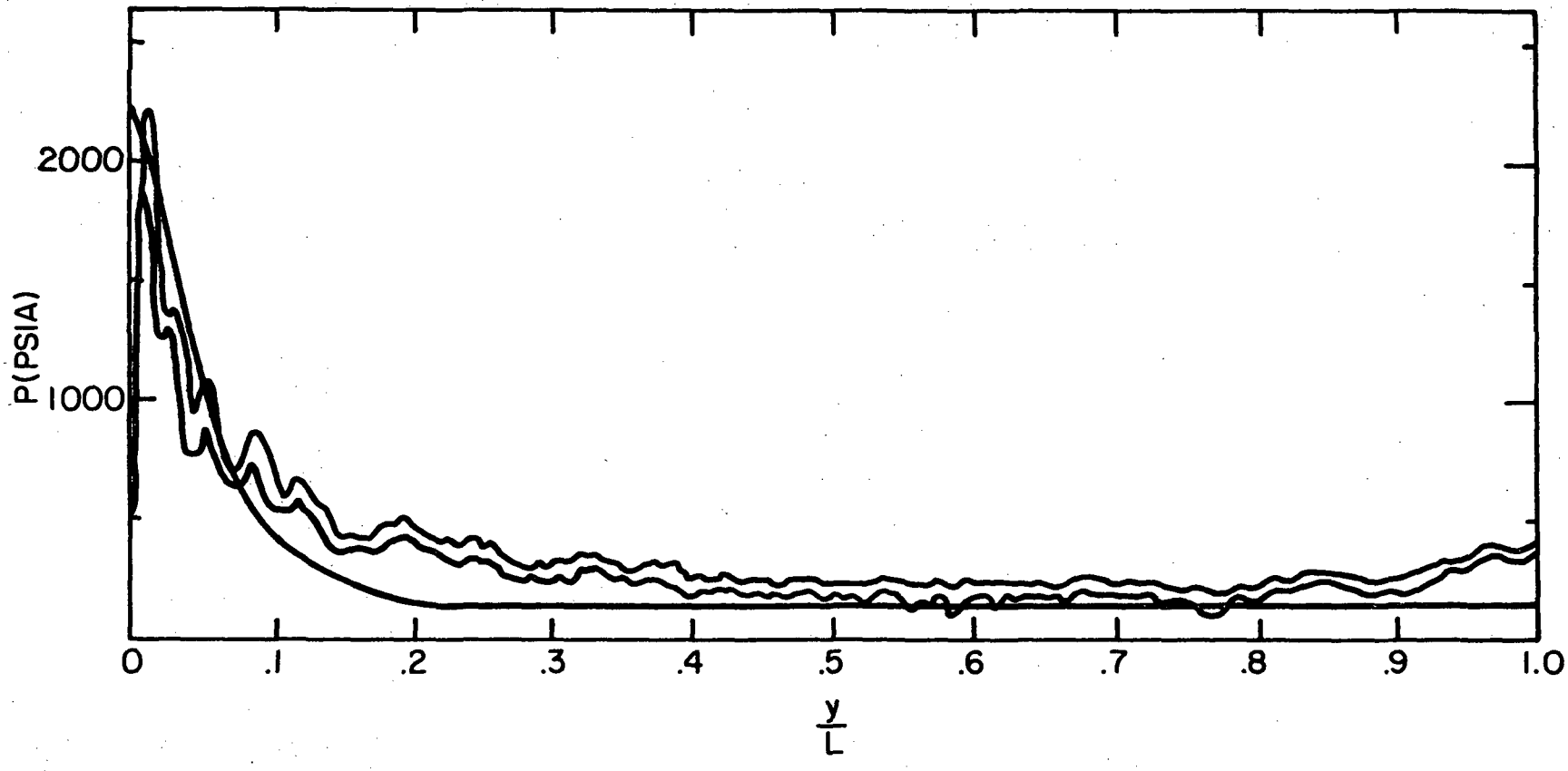


Fig. 8. Comparison of Actual and Calculated Pressure Distributions Along the Injector Plate for Run 956 of Ref. 11.

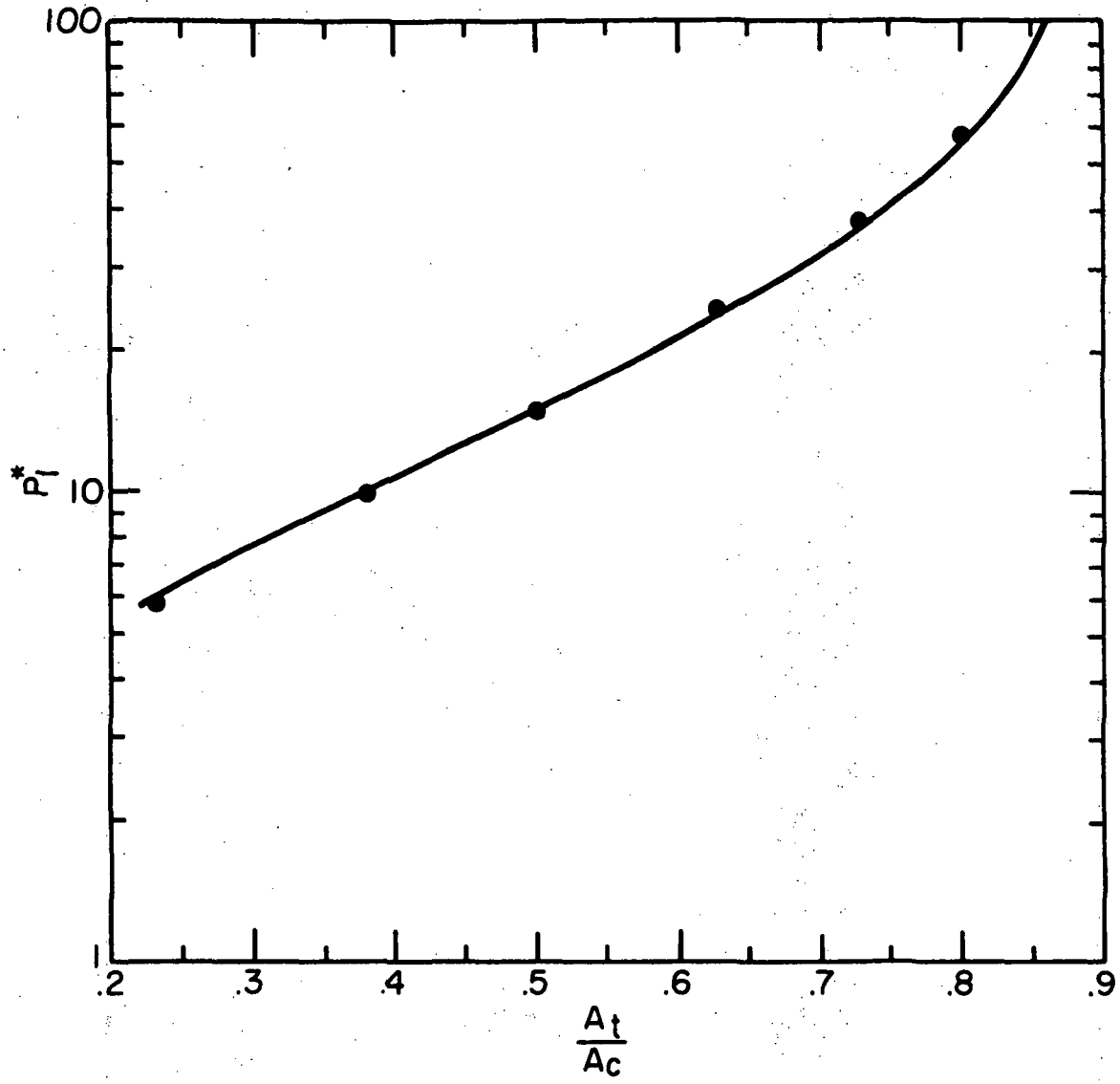


Fig. 9. $P_1^*$ versus $A_t/A_c$ for $x_d/L$ = constant = 0.0575 and T = 1.26. The Points Indicated by ● Show the Very Small Changes which Occur when an $x_d/L$ which Varies According to Eq. (18) is employed.

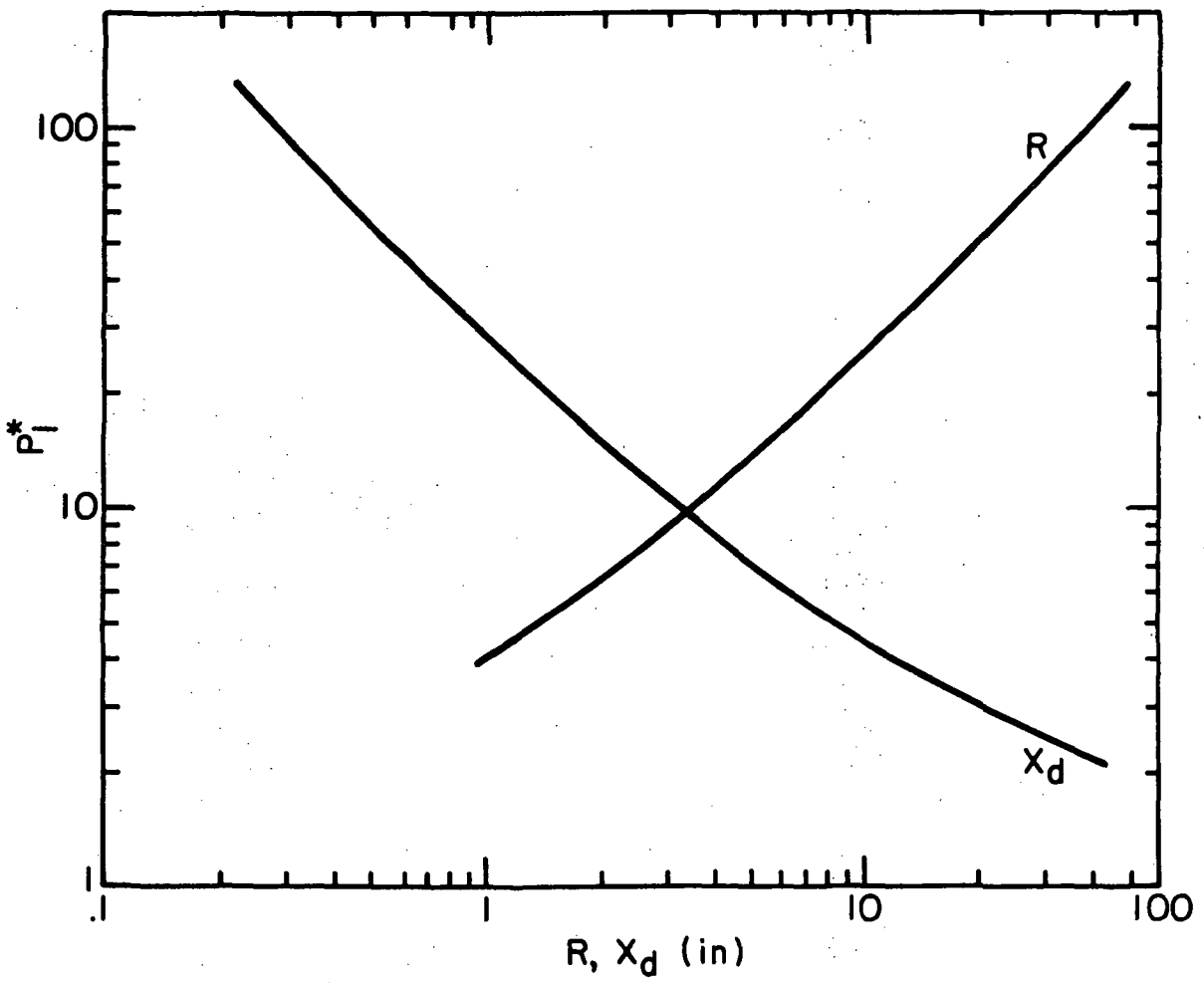


Fig. 10. $P_1^*$ versus $x_d$ and R for $\gamma = 1.26$ and $A_t/A_c = 1/2$ ($z = 0.2796$). Calculations for $x_d$ were made Assuming a 5.5 in. Radius Motor, as in Ref. 11, so that L = 34.54 in. Calculations for R were made Assuming $x_d = 1.988$ in., corresponding to the numbers in the Example Calculation in the Test. ($x_d/L = 0.0575$)

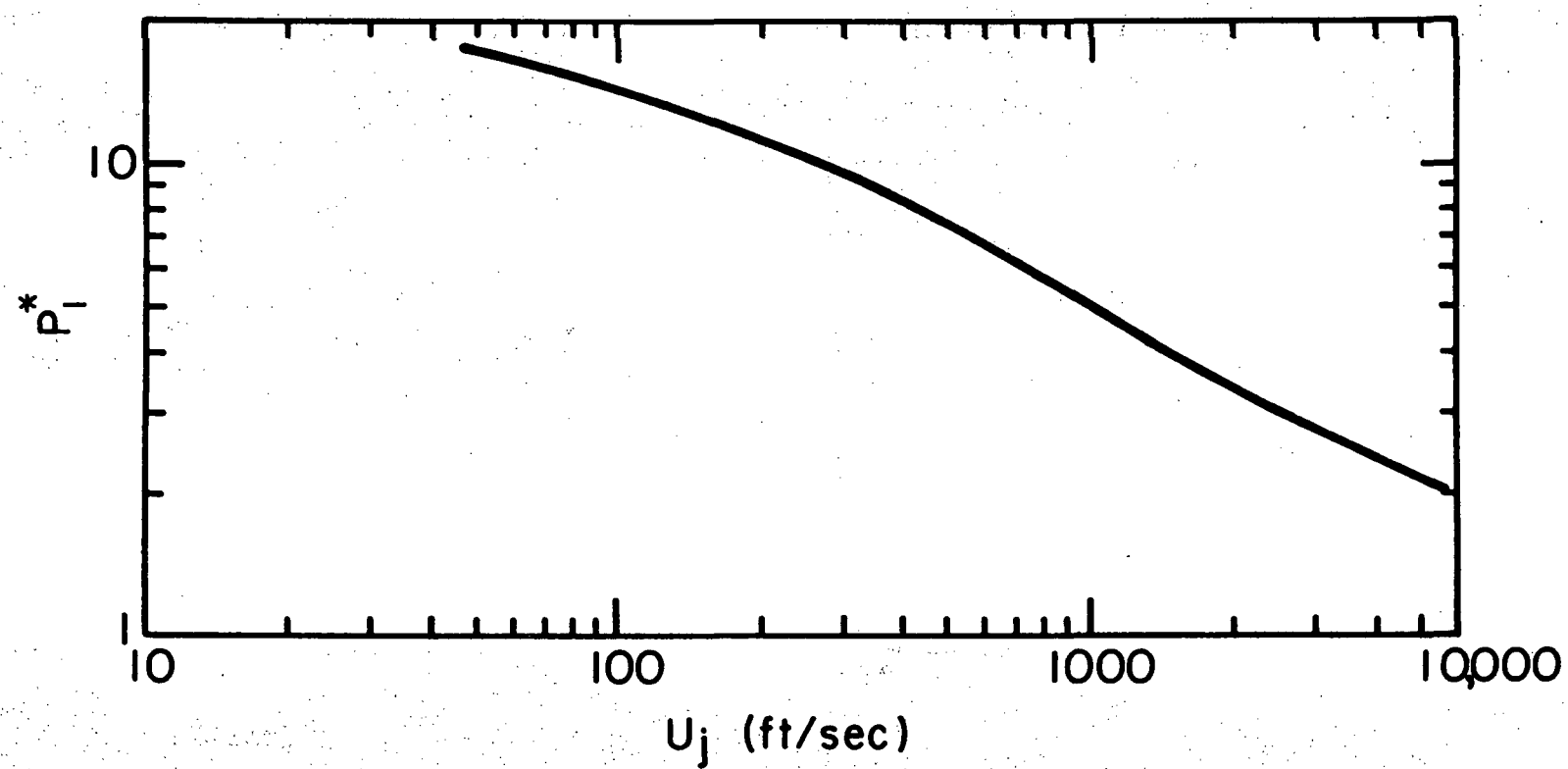


Fig. 11. $P_1^*$ versus $u_j$, for $\gamma = 1.26$, $x_i/L = 0.75/34.54 = 0.0432$, and $A_c = 3530$ ft/sec (Re. Eq. (16)).

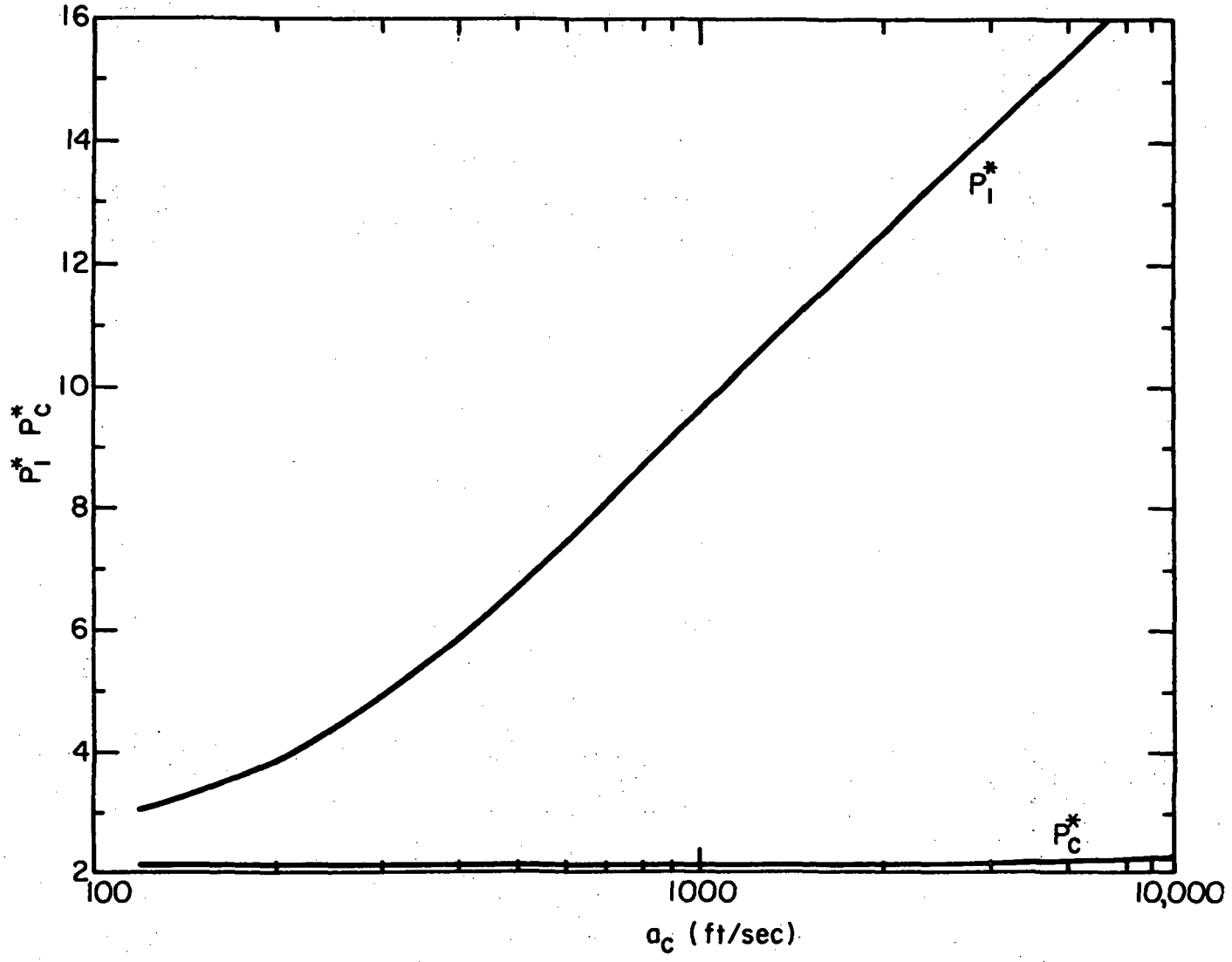


Fig. 12. $P_1^*$ and $P_c^*$ versus $A_c$ for $\gamma = 1.26$, $A_t/A_c = 1/2$, ($z = 0.2796$), $u_j = 93.6$ ft/sec, and $x_i/L = 0.0432$.

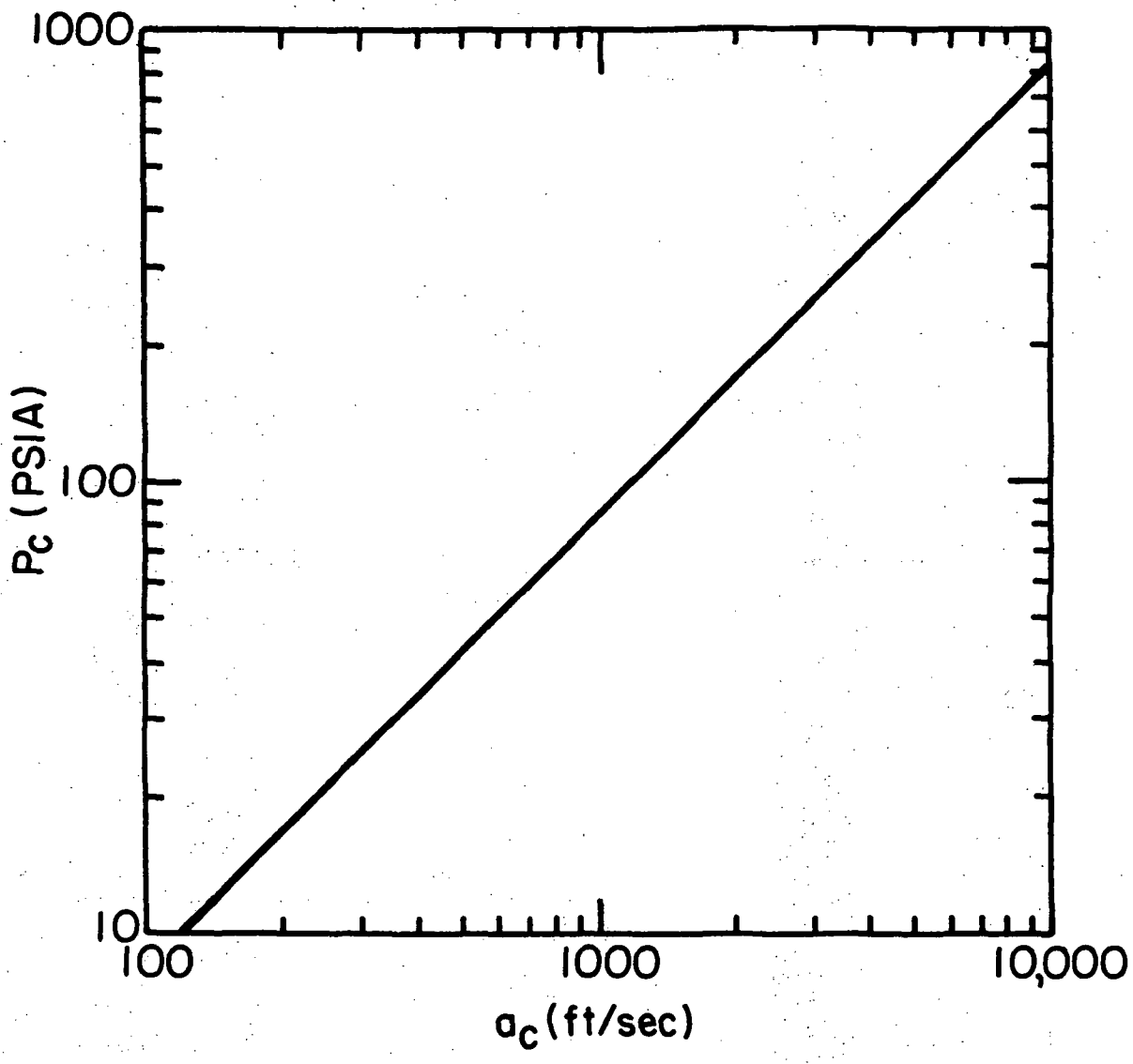


Fig. 13. $P_c$ versus $A_c$ for Same Conditions as in Fig. 12 and $\dot{m}_p / A_c$ = 1 lbm/ in.$^2$ sec.

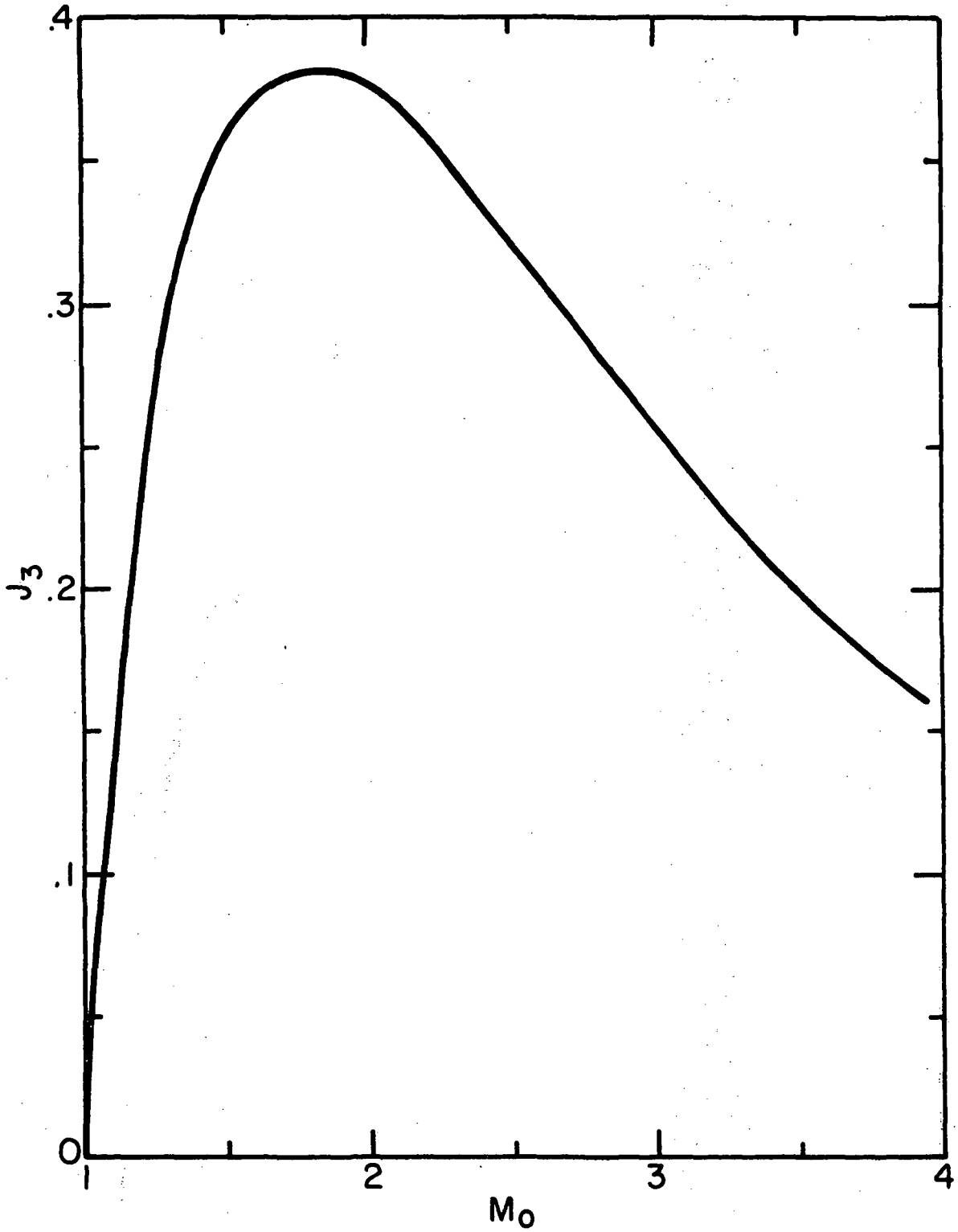


Fig. 14. $J_3$ versus $M_o$ for $\gamma = 1.26$.

Dr. R.J. Priem MS 500-209
NASA Lewis Research Center
21000 Brookpark Road
Cleveland, Ohio 44135 (2)

NASA-Lewis Research Center
Attention: N.T. Musial (M.S. 500-311)
21000 Brookpark Road
Cleveland, Ohio 44135

NASA-Lewis Research Center
Attention: Library (M.S. 60-3)
21000 Brookpark Road
Cleveland, Ohio 44135

NASA-Lewis Research Center
Attention: Report Control Office (M.S. 5-5)
21000 Brookpark Road
Cleveland, Ohio 44135

Brooklyn Polytechnic Institute
Attn: V.D. Agosta
Long Island Graduate Center
Route 110
Farmingdale, New York 11735

Chemical Propulsion Information Agency
Johns Hopkins University/APL
Attn: T.W. Christian
8621 Georgia Avenue
Silver Spring, Maryland 20910

NASA Lewis Research Center
Attn: E.W. Conrad, MS 500-204
21000 Brookpark Road
Cleveland, Ohio 44135

Aerospace Corporation
Attn: O.W. Dykema
Post Office Box 95085
Los Angeles, California 90045

Ohio State University
Department of Aeronautical and Astronautical Engineering
Attn: R. Edse
Columbus, Ohio 43210

TRW Systems
Attn: G.W. Elverum
One Space Park
Redondo Beach, California 90278

Bell Aerospace Company
Attn: T.F. Ferger
Post Office Box 1
Mail Zone J-81
Buffalo, New York 14205

Pratt & Whitney Aircraft
Florida Research & Development Center
Attn: G.D. Garrison
Post Office Box 710
West Palm Beach, Florida 33402

NASA Lewis Research Center
Attn: L. Gordon, MS 500-209
21000 Brookpark Road
Cleveland, Ohio 44135

Purdue University
School of Mechanical Engineering
Attn: R. Goulard
Lafayette, Indiana 47907

North American Rockwell Corporation
Rocketdyne Division
Attn: L. P. Combs, D/991-350
Zone 11
6633 Canoga Avenue
Canoga Park, California 91304

NASA Scientific and Technical
Information Facility (10 copies)
Attention: Acquisitions Branch
P.O. Box 33
College Park, Maryland 20740

University of Illinois
Aeronautics/Astronautic Engineering
Department
Attn: R.A. Strehlow
Transportation Building, Room 101
Urbana, Illinois 61801

NASA
Manned Spacecraft Center
Attn: J.G. Thibadaux
Houston, Texas 77058

Massachusetts Institute of Technology
Department of Mechanical Engineering
Attn: T.Y. Toong
77 Massachusetts Avenue
Cambridge, Massachusetts 02139

Illinois Institute of Technology
Attn: T.P. Torda
Room 200 M.H.
3300 S. Federal Street
Chicago, Illinois 60616

AFRPL
Attn: R.R. Weiss
Edwards, California 93523

U.S. Army Missile Command
AMSMI-RKL, Attn: W.W. Wharton
Redstone Arsenal, Alabama 35808

Air Force Office of Scientific
Chief Propulsion Division
Attn: Let. Col. R.W. Haffner (NAE)
1400 Wilson Boulevard
Arlington, Virginia 22209

Pennsylvania State University
Mechanical Engineering Department
Attn: G.M. Faeth
207 Mechanical Engineering Bldg.
University Park, Pennsylvania 16802

TISIA
Defense Documentation Center
Cameron Station
Building 5
5010 Duke Street
Alexandria, Virginia 22314

Office of Assistant Director
(Chemical Technician)
Office of the Director of Defense
Research and Engineering
Washington, D.C. 20301

D.E. Mock
Advanced Research Projects Agency
Washington, D.C. 20525

Dr. H.K. Doetsch
Arnold Engineering Development Center
Air Force Systems Command
Tullahoma, Tennessee 37389

Library
Air Force Rocket Propulsion Laboratory
(RPR)
Edwards, California 93523

Library, Bureau of Naval Weapons
Department of the Navy
Washington, D.C.

U.S. Army Missile Command
AMSMI-RKL, Attn: W.W. Wharton
Redstone Arsenal, Alabama 35808

University of California
Aerospace Engineering Department
Attn: F.A. Williams
Post Office Box 109
LaJolla, California 92037

Georgia Institute of Technology
Aerospace School
Attn: B.T. Zinn
Atlanta, Georgia 30332

Marshall Industries
Dynamic Science Division
2400 Michelson Drive
Irvine, California 92664

Mr. Donald H. Dahlene
U.S. Army Missile Command
Research, Development, Engineering
and Missile Systems Laboratory
Attn: AMSMI-RK
Redstone Arsenal, Alabama 35809

Princeton University
James Forrestal Campus Library
Attn: D. Harrje
Post Office Box 710
Princeton, New Jersey 08540

U.S. Naval Weapons Center
Attn: T. Inouye, Code 4581
China Lake, California 93555

Office of Naval Research
Navy Department
Attn: R.D. Jackel, 473
Washington, D.C. 20360

Library
Director (Code 6180)
U.S. Naval Research Laboratory
Washington, D.C. 20390

APRP (Library)
Air Force Aero Propulsion Laboratory
Research and Technology Division
Air Force Systems Command
United States Air Force
Wright-Patterson AFB, Ohio 45433

Technical Information Department
Aeronutronic Division of Philco Ford
Corporation
Ford Road
Newport Beach, California 92663

Library-Documents
Aerospace Corporation
2400 E. El Segundo Boulevard
Los Angeles, California 90045

University of Michigan
Aerospace Engineering
Attn: J. A. Nicholls
Ann Arbor, Michigan 48105

Tulane University
Attn: J.C. O'Hara
6823 St. Charles Avenue
New Orleans, Louisiana 70118

University of California
Department of Chemical Engineering
Attn: A.K. Oppenheim
6161 Etcheverry Hall
Berkeley, California 94720

Sacramento State College
School of Engineering
Attn: F.H. Reardon
6000 J. Street
Sacramento, California 95819

Air Force Aero Propulsion Laboratory
Attn: APTC Lt. M. Johnson
Wright-Patterson AFB, Ohio 45433

Naval Underwater Systems Center
Energy Conversion Department
Attn: Dr. R.S. Lazar, Code TB 131
Newport, Rhode Island 02840

NASA
Langley Research Center
Attn: R.S. Levine, MS 213
Hampton, Virginia 23365

Aerojet General Corporation
Attn: David A. Fairchild, Mech. Design
Post Office Box 15847 (Sect. 9732)
Sacramento, California 95809

Colorado State University
Mechanical Engineering Department
Attn: C.E. Mitchell
Fort Collins, Colorado 80521

University of Wisconsin
Mechanical Engineering Department
Attn: P.S. Myers
1513 University Avenue
Madison, Wis consin 53706

North American Rockwell Corporation
Rocketdyne Division
Attn: J.A. Nestlerode,
AC46 D/596-121
6633 Canoga Avenue
Canoga Park, California 91304

Library
Bell Aerosystems, Inc.
Box 1
Buffalo, New York 14205

Purdue University
School of Mechanical Engineering
Attn: B.A. Reese
Lafayette, Indiana 47907

NASA
George C. Marshall Space Flight Center
Attn: R.J. Richmond, SNE-ASTN-PP
Huntsville, Alabama 35812

Jet Propulsion Laboratory
California Institute of Technology
Attn: J.H. Rupe
4800 Oak Grove Drive
Pasadena, California 91103

University of California
Mechanical Engineering Thermal Systems
Attn: Prof. R. Sawyer
Berkeley, California 94720

ARL (ARC)
Attn: K. Scheller
Wright-Patterson AFB, Ohio 45433

Library
Susquehanna Corporation
Atlantic Research Division
Shirley Highway and Edsall Road
Alexandria, Virginia 22314

STL Tech. Lib. Doc. Acquisitions
TRW Systems Group
One Space Park
Redondo Beach, California 90278

Dr. David Altman
United Aircraft Corporation
United Technology Center
Post Office Box 358
Sunnyvale, California 94088

Report Library, Room 6A
Battelle Memorial Institute
505 King Avenue
Columbus, Ohio 43201

D. Suichu
General Electric Company
Flight Propulsion Laboratory Department
Cincinnati, Ohio 45215

Library
Ling-Temco-Vought Corporation
Post Office Box 5907
Dallas, Texas 75222

Marquardt Corporation
16555 Saticoy Street
Box 2013 - South Annex
Van Nuys, California 91409

P. F. Winternitz
New York University
University Heights
New York, New York

R. Stiff
Propulsion Division
Aerojet-General Corporation
Post Office Box 15847
Sacramento, California 95803

Library, Department 596-306
Rocketdyne Division of Rockwell
North American Rockwell Inc.
6633 Canoga Avenue
Canoga Park, California 91304

Library
Stanford Research Institute
333 Ravenswood Avenue
Menlo Park, California 94025

Library
United Aircraft Corporation
Pratt and Whitney Division
Florida Research and Development Center
Post Office Box 2691
West Palm Beach, Florida 33402

Library
Air Force Rocket Propulsion Laboratory (RPM)
Edwards, California 93523

Kenneth R. Purdy, Professor
Post Office Box 5014
Tennessee Technological University
Cookeville, Tennessee 38501

NASA
Lewis Research Center
Attn: E. O. Bourke MS 500-209
21000 Brookpark Road
Cleveland, Ohio 44135

NASA
Lewis Research Center MS 500-313
Rockets & Spacecraft Procurement Section
21000 Brookpark Road
Cleveland, Ohio 44135

| 1. Report No. | 2. Government Accession No. | 3. Recipient's Catalog No. |
|---|---|---|
| NASA CR 121194 | | |

| 4. Title and Subtitle | 5. Report Date |
|---|---|
| THEORETICAL ANALYSIS OF A ROTATING TWO PHASE DETONATION IN A ROCKET MOTOR | May 1973 |
| | 6. Performing Organization Code |

| 7. Author(s) | 8. Performing Organization Report No. |
|---|---|
| I-wu Shen and T.C. Adamson, Jr. | |
| | 10. Work Unit No. |

| 9. Performing Organization Name and Address | 11. Contract or Grant No. |
|---|---|
| The University of Michigan<br>Department of Aerospace Engineering<br>Gas Dynamics Laboratories<br>Ann Arbor, Michigan 48105 | NGL 23-005-336 |
| | 13. Type of Report and Period Covered |
| 12. Sponsoring Agency Name and Address | Contractor Report |
| National Aeronautics and Space Administration<br>Washington, D.C. 20546 | 14. Sponsoring Agency Code |

15. Supplementary Notes

Project Manager, Richard J. Priem, Chemical Propulsion Division
NASA Lewis Research Center, Cleveland, Ohio

16. Abstract

Tangential mode, non-linear wave motion in a liquid propellant rocket engine is studied, using a two phase detonation wave as the reaction model. Because the detonation wave is followed immediately by expansion waves, due to the side relief in the axial direction, it is a Chapman-Jouguet wave. The strength of this wave, which may be characterized by the pressure ratio across the wave, as well as the wave speed and the local wave Mach number, are related to design parameters such as the contraction ratio, chamber speed of sound, chamber diameter, propellant injection density and velocity, and the specific heat ratio of the burned gases. In addition, the distribution of flow properties along the injector face can be computed. Numerical calculations show favorable comparison with experimental findings. Finally, the effects of drop size are discussed and a simple criterion is found to set the lower limit of validity of this "strong wave" analysis.

| 17. Key Words (Suggested by Author(s)) | 18. Distribution Statement |
|---|---|
| Detonation<br>Rocket Motor Combustion<br>Combustion Instability | Unclassified - unlimited |

| 19. Security Classif. (of this report) | 20. Security Classif. (of this page) | 21. No. of Pages | 22. Price* |
|---|---|---|---|
| Unclassified | Unclassified | | |

*For sale by the National Technical Information Service, Springfield, Virginia 22151